



**NAVAL
POSTGRADUATE
SCHOOL**

MONTEREY, CALIFORNIA

THESIS

**MICROSTRUCTURAL EFFECTS OF MULTIPLE PASSES
DURING FRICTION STIR PROCESSING OF NICKEL
ALUMINUM BRONZE**

by

Elizabeth A. Nelson

December 2009

Thesis Advisor:
Second Reader:

Terry R. McNelley
Sarath Menon

Approved for public release; distribution is unlimited

REPORT DOCUMENTATION PAGE			<i>Form Approved OMB No. 0704-0188</i>
Public reporting burden for this collection of information is estimated to average 1 hour per response, including the time for reviewing instruction, searching existing data sources, gathering and maintaining the data needed, and completing and reviewing the collection of information. Send comments regarding this burden estimate or any other aspect of this collection of information, including suggestions for reducing this burden, to Washington headquarters Services, Directorate for Information Operations and Reports, 1215 Jefferson Davis Highway, Suite 1204, Arlington, VA 22202-4302, and to the Office of Management and Budget, Paperwork Reduction Project (0704-0188) Washington DC 20503.			
1. AGENCY USE ONLY (Leave blank)	2. REPORT DATE December 2009	3. REPORT TYPE AND DATES COVERED Master's Thesis	
4. TITLE AND SUBTITLE Microstructural Effects of Multiple Passes during Friction Stir Processing of Nickel Aluminum Bronze		5. FUNDING NUMBERS	
6. AUTHOR(S) Elizabeth A. Nelson		8. PERFORMING ORGANIZATION REPORT NUMBER	
7. PERFORMING ORGANIZATION NAME(S) AND ADDRESS(ES) Naval Postgraduate School Monterey, CA 93943-5000		10. SPONSORING/MONITORING AGENCY REPORT NUMBER	
9. SPONSORING /MONITORING AGENCY NAME(S) AND ADDRESS(ES) N/A		11. SUPPLEMENTARY NOTES The views expressed in this thesis are those of the author and do not reflect the official policy or position of the Department of Defense or the U.S. Government.	
12a. DISTRIBUTION / AVAILABILITY STATEMENT Approved for public release; distribution is unlimited		12b. DISTRIBUTION CODE A	
13. ABSTRACT (maximum 200 words) Friction Stir Processing (FSP) is an emerging technology based on Friction Stir Welding that allows the near surface regions of a material to be selectively processed to improve the material properties. Single and multiple pass samples of nickel aluminum bronze were examined and their microstructures studied and compared using optical microscopy and scanning electron microscopy. FSP conditions were 800 revolutions per minute (RPM), with a tool traversing speed of 101.6 mm per minute (4.0 inches per minute, or IPM), or 1200 RPM with 50.8 mm per minute (2.0 IPM). Quantitative microscopy methods were then employed to determine the approximate volume fraction of beta transformation products and the estimated peak temperatures at various points in the stir zones of the as-processed samples. The results showed that, in material that had undergone multiple, successive FSP passes, microstructural effects of the FSP include a refined, homogeneous grain size and a reduction in the volume fraction of beta transformation products when comparison is made to single pass material. The reduction in beta transformation products indicated that a reduction in the estimated peak temperature in the stir zone had occurred in the samples having undergone multiple FSP passes.			
14. SUBJECT TERMS Friction Stir Processing, Nickel Aluminum Bronze, Propellers, Microstructural Properties, Grain Refinement, Volume Fraction-Temperature Relationship			15. NUMBER OF PAGES 63
			16. PRICE CODE
17. SECURITY CLASSIFICATION OF REPORT Unclassified	18. SECURITY CLASSIFICATION OF THIS PAGE Unclassified	19. SECURITY CLASSIFICATION OF ABSTRACT Unclassified	20. LIMITATION OF ABSTRACT UU

THIS PAGE INTENTIONALLY LEFT BLANK

Approved for public release; distribution is unlimited

**MICROSTRUCTURAL EFFECTS OF MULTIPLE PASSES DURING FRICTION
STIR PROCESSING OF NICKEL ALUMINUM BRONZE**

Elizabeth A. Nelson
Lieutenant, United States Navy
B.S., United States Naval Academy, 2002

Submitted in partial fulfillment of the
requirements for the degree of

MASTER OF SCIENCE IN MECHANICAL ENGINEERING

from the

**NAVAL POSTGRADUATE SCHOOL
December 2009**

Author: Elizabeth A. Nelson

Approved by: Terry R. McNelley
Thesis Advisor

Sarath Menon
Second Reader

Knox T. Millsaps
Chairman, Department of Mechanical and Astronautical
Engineering

THIS PAGE INTENTIONALLY LEFT BLANK

ABSTRACT

Friction Stir Processing (FSP) is an emerging technology based on Friction Stir Welding that allows the near surface regions of a material to be selectively processed to improve the material properties. Single and multiple pass samples of nickel aluminum bronze were examined and their microstructures studied and compared using optical microscopy and scanning electron microscopy. FSP conditions were 800 revolutions per minute (RPM), with a tool traversing speed of 101.6 mm per minute (4.0 inches per minute, or IPM), or 1200 RPM with 50.8 mm per minute (2.0 IPM). Quantitative microscopy methods were then employed to determine the approximate volume fraction of beta transformation products and the estimated peak temperatures at various points in the stir zones of the as-processed samples. The results showed that, in material that had undergone multiple, successive FSP passes, microstructural effects of the FSP include a refined, homogeneous grain size and a reduction in the volume fraction of beta transformation products when comparison is made to single pass material. The reduction in beta transformation products indicated that a reduction in the estimated peak temperature in the stir zone had occurred in the samples having undergone multiple FSP passes.

THIS PAGE INTENTIONALLY LEFT BLANK

TABLE OF CONTENTS

I.	INTRODUCTION.....	1
II.	BACKGROUND INFORMATION	5
	A. FRICTION STIR PROCESSING	5
	B. NICKEL ALUMINUM BRONZE.....	5
III.	EXPERIMENTAL PROCEDURE.....	11
	A. OVERVIEW	11
	B. MATERIAL PROCESSING	11
	C. MICROSTRUCTURE ANALYSIS	13
	1. Optical Microscopy	13
	a. <i>Sample Preparation</i>	13
	b. <i>Optical Microscopy Procedure</i>	14
	2. Scanning Electron Microscope	16
	a. <i>Sample Preparation</i>	16
	b. <i>Scanning Electron Microscopy Procedure</i>	16
	D. VOLUME FRACTION DETERMINATION	17
	E. ESTIMATED PEAK TEMPERATURE DETERMINATION	18
IV.	RESULTS	19
	A. OVERVIEW	19
	B. OPTICAL MICROSCOPY.....	19
	C. VOLUME FRACTION DETERMINATION	24
	D. ESTIMATED PEAK TEMPERATURE DETERMINATION	26
V.	DISCUSSION	29
VI.	CONCLUSIONS	41
VII.	RECOMMENDATIONS FOR FUTURE WORK.....	43
	LIST OF REFERENCES.....	45
	INITIAL DISTRIBUTION LIST	47

THIS PAGE INTENTIONALLY LEFT BLANK

LIST OF FIGURES

Figure 1.	Friction stir processing illustration showing a) rotating tool with pin; b) application of pressure to force pin into work piece through adiabatic heating and softening; c) creation of the stir zone around the tool; d) traversing of tool through work piece. From [4].	2
Figure 2.	Example of an FSP stir zone; this is a transverse section and the tool traversing direction is normal to the image.	4
Figure 3.	Transformations product formation in nickel aluminum bronze. From [2].	7
Figure 4.	Optical micrograph taken at 50x magnification of as-cast nickel aluminum bronze showing α and κ phases (κ_i phase is not present).	8
Figure 5.	Scanning electron micrograph showing phases present in material which underwent multiple passes of FSP at a much finer scale than the as-cast material.	9
Figure 6.	Example of a rectangular spiral pattern used for FSP of multiple pass plates.	12
Figure 7.	Schematic showing location in SZ of optical microscopy surveys: a) locations for first survey; b) locations for second survey; c) locations for third survey and area used for optical montages; d) column locations for use in volume fraction and estimated peak temperature determinations.	15
Figure 8.	Scanning electron micrograph of an area which underwent FSP with an overlaid grid used for volume fraction determinations.	18
Figure 9.	Optical montages of micrographs from: a) Sample which underwent a single pass of FSP at 800/4; b) Sample which underwent multiple passes of FSP at 800/4.	21
Figure 10.	Optical montage of micrographs from: a) Sample which underwent a single pass of FSP at 1200/2; b) Sample which underwent multiple passes of FSP at 1200/2.	21
Figure 11.	Optical micrographs from 0.5 mm below surface of sample: a) 800/4 single pass column 4; b) 800/4 single pass column 7; c) 800/4 multiple passes column 5; d)800/4 multiple passes column 12.	22
Figure 12.	Optical micrographs from 5.3 mm below surface of sample: a) 800/4 single pass column 4; b) 800/4 single pass column 7; c) 800/4 multiple passes column 5; d)800/4 multiple passes column 12.	23
Figure 13.	Optical micrographs from 9.0 mm below surface of sample: a) 800/4 single pass column 4; b) 800/4 single pass column 7; c) 800/4 multiple passes column 5; d)800/4 multiple passes column 12.	23
Figure 14.	Volume fraction of α phase determinations for the samples having undergone FSP at a rotational speed of 800 RPM and a traversing rate of 4 IPM. In legend 's' signifies single pass sample, 'm' signifies multiple pass sample, and 'c' signifies the approximate column location.	25
Figure 15.	Volume fraction of α phase determinations for the samples having undergone FSP at a rotational speed of 1200 RPM and a traversing rate of 2 IPM. In legend 's' signifies single pass sample, 'm' signifies multiple pass sample, and 'c' signifies the approximate column location.	25
Figure 16.	SEM micrographs from multiple pass samples : a) 800/4 column 5; b) 800/4 column 12; c) 1200/2 column 5; d) 1200/2 column 12.	26

Figure 17.	Estimated peak temperature determinations for the samples having undergone FSP at a rotational speed of 800 RPM and a traversing rate of 4 IPM. In legend ‘s’ signifies single pass sample, ‘m’ signifies multiple pass sample, and ‘c’ signifies the approximate column location.....	27
Figure 18.	Estimated peak temperature determinations for the samples having undergone FSP at a rotational speed of 1200 RPM and a traversing rate of 2 IPM. In legend ‘s’ signifies single pass sample, ‘m’ signifies multiple pass sample, and ‘c’ signifies the approximate column location.....	27
Figure 19.	SEM montage of micrographs for 800 RPM and 4 IPM, single FSP pass sample, column 7.....	31
Figure 20.	SEM montage of micrographs for 800 RPM and 4 IPM, sample processed with multiple FSP passes, column 12.....	32
Figure 21.	SEM montage of micrographs for 1200 RPM and 2 IPM, single FSP pass sample, column 7.....	33
Figure 22.	SEM montage of micrographs for 1200 RPM and 2 IPM, sample processed with multiple FSP passes, column 12.....	34
Figure 23.	SEM micrographs for 1200 RPM and 2 IPM, 0.2 mm below sample surface: a) Single pass, Column 7, 300x magnification; b) Single pass, Column 7, 1500x magnification; c) Multiple pass, Column 12, 300x magnification; d) Multiple pass, Column 12, 1500x magnification.....	35
Figure 24.	Ultimate tensile strength and elongation data for sample which underwent a single pass of FSP at 1000 RPM and 4 IPM with a 13 mm tool diameter. From [12]......	36
Figure 25.	Mechanical property data for multiple pass region in material which underwent FSP with multiple passes. RPM-IPM combinations given in legends. From [10]......	38

LIST OF TABLES

Table 1.	ASTM Standard B148, Standard Specification for Aluminum–Bronze Sand Castings. From [9].	6
Table 2.	Composition data (wt%). From [15].	13

THIS PAGE INTENTIONALLY LEFT BLANK

ACKNOWLEDGMENTS

I would like to start off by thanking my thesis advisor, Dr. Terry McNelley, for all the discussions and guidance; this truly was a great experience. I would like to thank Dr. Sarath Menon for additional guidance and for taking the time to tutor me on the use of the SEM. I would like to thank Dr. Jianqing Su for helping me to get started and teaching me how to prepare the samples.

I would also like to thank my husband, Daniel, whose moral support was a necessary ingredient in my success. I would like to thank my cats, Spooky and Melvin, who are always bright stars in gloomy skies.

Additionally, I would like to thank my parents, who have always motivated me to do better.

THIS PAGE INTENTIONALLY LEFT BLANK

I. INTRODUCTION

Friction Stir Processing (FSP) is a promising technology that can improve material properties and that has an application in the processing of marine propellers. Many marine propellers, including those in use by the U.S. Navy, are made using nickel aluminum bronze, a Cu-9Al-5Ni-4Fe alloy (nominal composition in weight percent). Nickel aluminum bronze combines good casting characteristics with moderate strength, good fatigue resistance, and fracture toughness, as well as corrosion resistance in a marine environment.

In casting a nickel aluminum bronze propeller, several issues are of concern. Due to the variable thicknesses in propellers from the blade tip to the blade root and base, variable cooling rates are encountered, leading to a variability in microstructure. Overall slow cooling rates result in coarse microstructures with reduced mechanical properties [1]. Also, significant porosity is encountered in as-cast nickel aluminum bronze. Currently, propeller manufacturing requires the use of fusion welds to repair these porosity defects. Once a fusion weld repair is completed, the area needs to be machined to restore a smooth surface. As more porosity is uncovered, repeating cycles of fusion welding and machining lead to high costs and extended manufacturing and repair periods [2]. FSP of the propeller surface can create a layer of refined, homogeneous microstructure, with the elimination of porosity, over the entire exterior of the propeller or only a selected area of the propeller, and thereby improve the surface's mechanical properties and thus service performance of the propeller.

FSP is an allied technology of Friction Stir Welding (FSW). FSW, which was originally developed at The Welding Institute in Cambridge, England, is a solid state welding process wherein the work pieces to be joined are rigidly clamped together and then a rotating cylindrical tool with a projecting pin is plunged into the work pieces and traversed along the weld line. Since this is a solid state process, the work pieces never achieve temperatures in excess of their liquidus temperatures and, since no filler material is used the chemical composition of the weld is determined only by the base metal(s).

The tool is able to plunge into the work pieces due to heating resulting from sliding friction and compression of the tool against the surface of the material and plastic deformation leading to adiabatic heating and local softening [3]. In FSP, again, a cylindrical tool with a projecting pin is rotated, plunged, and traversed through metal, though now in order to improve the material properties of the surface of that metal. A FSP illustration is shown in Figure 1.

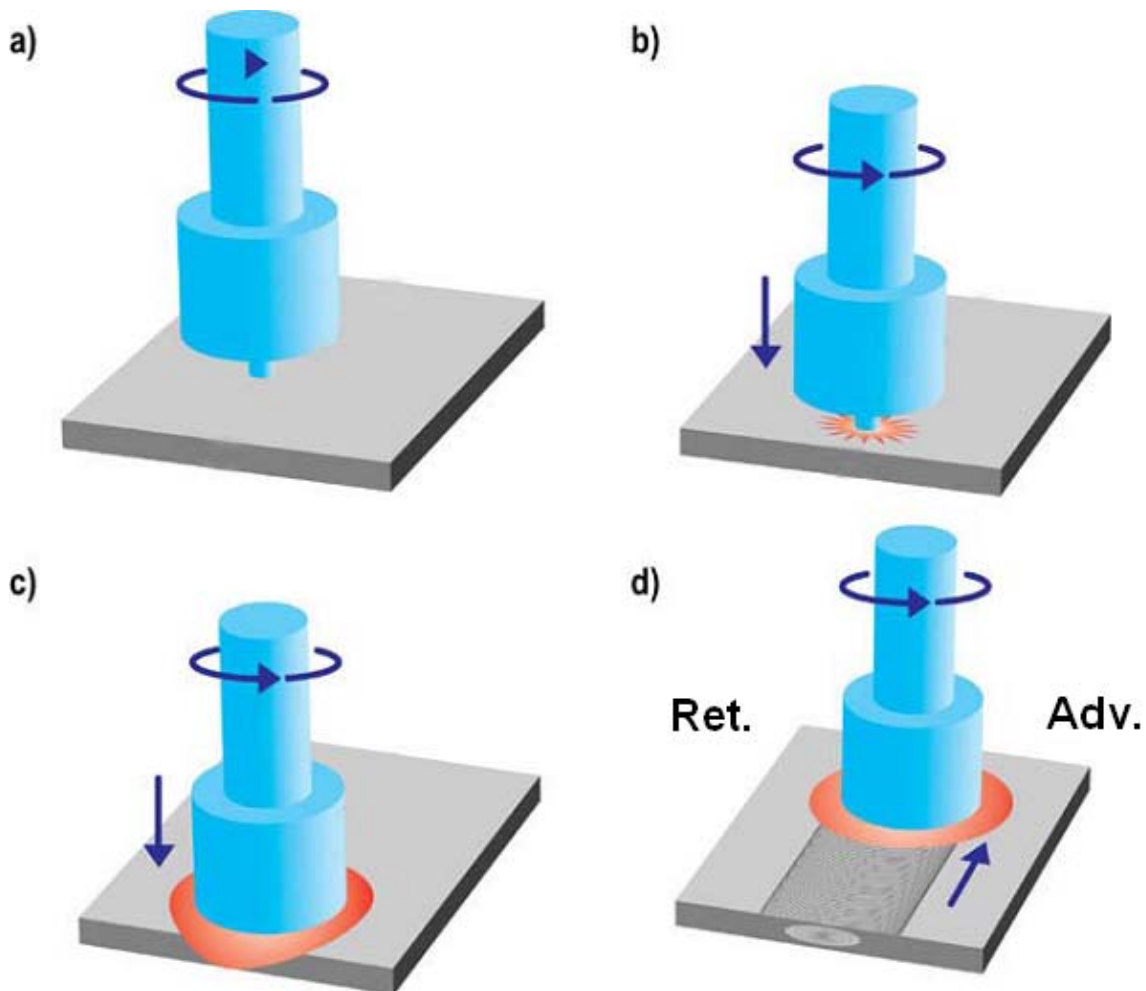


Figure 1. Friction stir processing illustration showing a) rotating tool with pin; b) application of pressure to force pin into work piece through adiabatic heating and softening; c) creation of the stir zone around the tool; d) traversing of tool through work piece. From [4].

The FSP tool is cylindrical in shape with a smaller diameter projecting pin which may have threads, a stepped diameter, or flutes. The tool is made from various wear resistant materials, depending on the material to be processed, in order to prevent erosion of the tool and contamination of the processed area. Tool materials have included various tool steel compositions for use with aluminum, and materials such as Densimet®, a tungsten-iron composite. Additionally, various other tungsten-based alloys have been used with copper-based and titanium-based alloys. When the tool is forced into the surface of the material, the pin is submerged completely and the shoulder of the tool comes into contact with the surface of the metal. The shoulder restricts the upward movement of the material and therefore limits the flow to the horizontal and vertical direction around the pin. This restriction and the rotation of the tool and pin create a heating effect and a stirring action in the material, which results in homogenous mixing and grain refinement.

The movement of the metal around the pin creates a region of severe plastic deformation of material called the stir zone (SZ). The size and shape of the SZ is highly dependent on the FSP parameters used, such as the tool size, pin size and shape, tool rotational speed, and tool traversing rate. In the SZ, the large deformations due to the movement around the pin along with the frictional and adiabatic heating result in a very refined, homogeneous microstructure with a reduction in gas porosity and inclusion redistribution. In this region, large gradients in strains, strain rates, and temperatures have also been noted with steeper gradients forming on the advancing side of the tool [5]. This has shown to yield improved material properties such as increased strength and ductility and improved corrosion resistance, as well as surface hardening and conversion of microstructures to a wrought condition in the absence of shape change in cast components. Just outside the SZ is the thermo-mechanically affected zone (TMAZ). In this region, the work piece undergoes less heating and plastic deformation as can be seen by the distortion and elongation of base metal grains. Just outside the TMAZ is the heat affected zone (HAZ). Here, the remaining heat from FSP has altered the microstructure and mechanical properties of the base metal, though there is no plastic deformation. These regions can be seen in Figure 2.

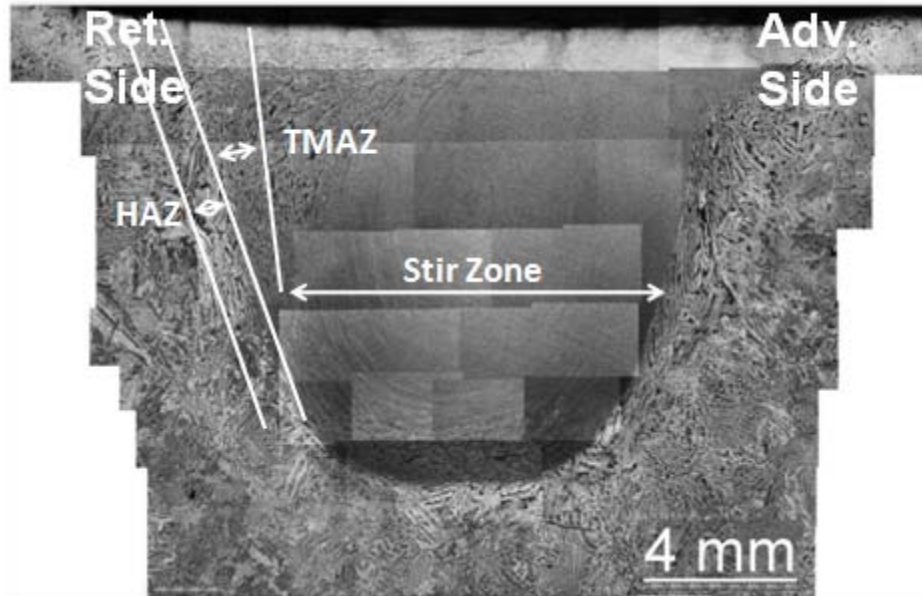


Figure 2. Example of an FSP stir zone; this is a transverse section and the tool traversing direction is normal to the image.

Also seen in Figure 2 are the differences between the advancing (right side) and retreating (left side) sides of the tool. On the advancing side, the tool is traveling in the same direction as it is rotating and a clear boundary is seen between the SZ and the TMAZ. On the retreating side, this boundary is more diffuse and a more gradual transition is made between the SZ and the TMAZ.

II. BACKGROUND INFORMATION

A. FRICTION STIR PROCESSING

To this date, FSP and FSW have been used most extensively on aluminum-based alloys, wherein fusion welding is difficult, though these technologies have also been applied to iron, titanium, copper, magnesium, and nickel based alloys. They have been shown to create uniform particle distributions, elimination of porosity, and highly refined grains. Such improved microstructures may produce significant surface hardening and may even support high strain rate superplasticity. FSP of aluminum and its alloys has been used specifically for microstructural modification, to increase superplasticity, to create surface composites, to homogenize composites, and to refine microstructures [6].

Past research on FSP of nickel aluminum bronze at NPS has accomplished several things. Among them are that comparisons have been made between fusion welding and FSP, relationships have been determined concerning microstructural effects due to variations in FSP parameters and correlations have been established between the microstructure and the mechanical properties of samples which have undergone both single and multiple passes. Of particular importance is that methods to estimate local peak SZ temperatures have been developed. These methods rely on quantitative analysis of SZ microstructures. The purpose of the current research was to determine the differences between the microstructure of samples having undergone a single FSP pass and samples having undergone multiple passes, and, ultimately, to determine the differences between the estimated peak temperatures by analysis of volume fractions of β transformation products in the samples.

B. NICKEL ALUMINUM BRONZE

Nickel aluminum bronze is a material that has an evolved composition. The binary copper-aluminum system has an intermetallic phase which is prone to selective attack and therefore yields increased corrosion. The addition of nickel and iron alloying

elements to the copper–aluminum system creates new intermetallic phases and suppresses the formation of the corrosion susceptible copper-aluminum phase [7].

Nickel aluminum bronze is widely used in marine applications because of this good resistance to sea water corrosion combined with moderate strength, ease of casting, low magnetic permeability, and good resistance to shock [8]. Nickel aluminum bronze for cast marine propellers falls under the American Society for Testing and Materials (ASTM) standard B148, Standard Specification for Aluminum–Bronze Sand Castings, for copper alloy UNS C95800 listed in Table 1.

Element	Cu	Ni	Fe	Al	Si	Mn
Nominal Composition, %	81.3	4.5	4.0	9.0	-	1.2

Table 1. ASTM Standard B148, Standard Specification for Aluminum–Bronze Sand Castings. From [9].

Casting of a propeller involves melting of the nickel aluminum bronze and pouring into a sand mold. It then solidifies at 1070 °C, cooling slowly ($\sim 10^{-3} \text{ }^\circ\text{C s}^{-1}$) to ambient temperature. During this time, the nickel aluminum bronze undergoes several microstructural changes as can be seen by the equilibrium cooling path in Figure 3. First, it remains entirely β phase until it is cooled below 1030 °C. Then the primary α phase forms in the β phase with a Widmanstätten morphology. At temperatures below 930 °C, globular κ_{ii} phase begins to form in the β phase. If there is greater than five weight percent iron, the κ_i phase forms. When the temperature falls to 860 °C, κ_{iv} phase starts to form in the α phase as the solubility of iron is exceeded. At 800 °C, the remaining β phase is transformed into κ_{iii} phase through the eutectoid reaction, $\beta \rightarrow \alpha + \kappa_{iii}$. Once the casting is at room temperature, the bronze consists entirely of α phase and the κ phases, i.e., β transformation products formed during near equilibrium cooling [10]. An optical micrograph showing the α and κ phases in the as–cast nickel aluminum bronze can be seen in Figure 4.

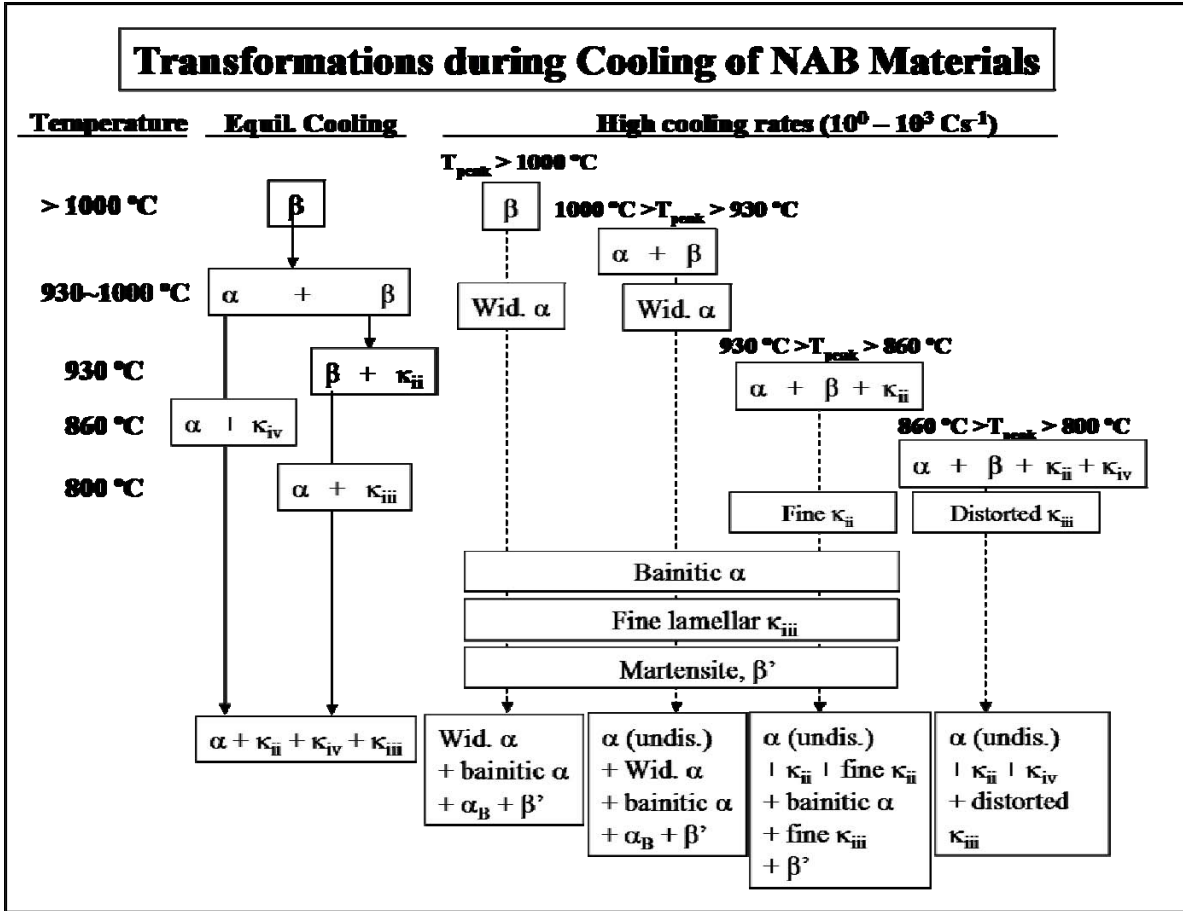


Figure 3. Transformations product formation in nickel aluminum bronze. From [2].

The β phase is a body centered cubic (BCC) solid solution with a lattice parameter of 0.357 nm. This phase is stable only at temperatures above the eutectoid temperature which is approximately 800 °C. Upon cooling the β phase transforms into the α phase and the κ phases, though the transformation products of the β phase depend on cooling rate. At higher cooling rates, some β phase may remain, which has been termed retained β (or β'), and has an ordered 3R or 2H martensitic structure with a high density of NiAl precipitates [11]. This retained β phase has a negative effect on the corrosion resistance of nickel aluminum bronze in sea water; therefore, to ensure that no retained β phase remains, either slow cooling rates are necessary or post casting tempering needs to be completed.

The primary α phase is a face centered cubic (FCC) solid solution with a lattice parameter of 0.364 nm. This phase is rich in copper with small amounts of aluminum,

nickel, iron, and manganese. The temperature at which this phase is manifested is highly dependent on the amount of aluminum in the base metal, with a lower amount of aluminum yielding a higher formation temperature. The temperature at which the α phase forms affects the amount of iron in the phase, and therefore, the centers of the α grains usually have the highest iron content and are the locations for κ_{iv} nucleation [12].

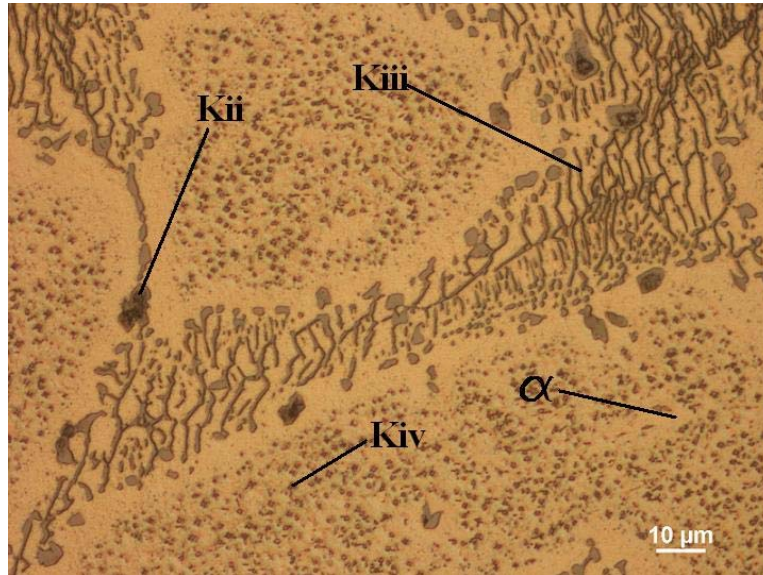


Figure 4. Optical micrograph taken at 50x magnification of as-cast nickel aluminum bronze showing α and κ phases (κ_i phase is not present).

In high iron alloys, the κ_i phase is seen in the center of the α phase with a large, rosette shaped morphology typically 20 to 50 μm in diameter. This phase is nominally Fe_3Al formed around a small copper rich particle with small amounts of nickel, silicon, and manganese. This phase is very sensitive to alloy (iron) content and cooling rate [13].

The κ_{ii} phase is globular in nature and has a DO_3 structure with a lattice parameter of 0.577 nm. This phase is much finer than the κ_i phase with a 5 to 10 μm diameter. The κ_{ii} phase is nominally Fe_3Al with small amounts of copper, silicon, nickel, and manganese. The κ_{ii} phase nucleates in the β phase and is therefore found in the areas containing the κ_{iii} phase, though occasionally while the α phase was growing it enveloped some of the κ_{ii} phase which had formed at the α/β interface.

The κ_{iii} phase has an ordered BCC (B2) structure with a lattice parameter of 0.288. This phase is nominally NiAl with small amounts of copper, iron, and manganese.

It has a lamellar morphology and forms as the eutectoid decomposition product, though a proeutectoid κ_{iii} phase may also form in a globular morphology.

The κ_{iv} phase is very similar to the κ_{ii} phase, having a DO_3 structure with a lattice parameter of 0.577 nm. It is nominally Fe_3Al with small amounts of silicon, nickel, manganese, and copper and forms as fine precipitates in the α phase [14].

During FSP, significantly faster cooling rates are seen and the transformation upon cooling follows one of the paths on the right side of Figure 3. Determination of which path is followed depends on the peak temperature seen by the material which undergoes FSP. An example of the microstructure present after multiple passes of FSP is seen in the scanning electron micrograph in Figure 5. In this micrograph the α phase is the dark constituent while the β transformation products are the light etching. Similar features are shared between Figures 4 and 5, though Figure 5 is at a much finer scale.

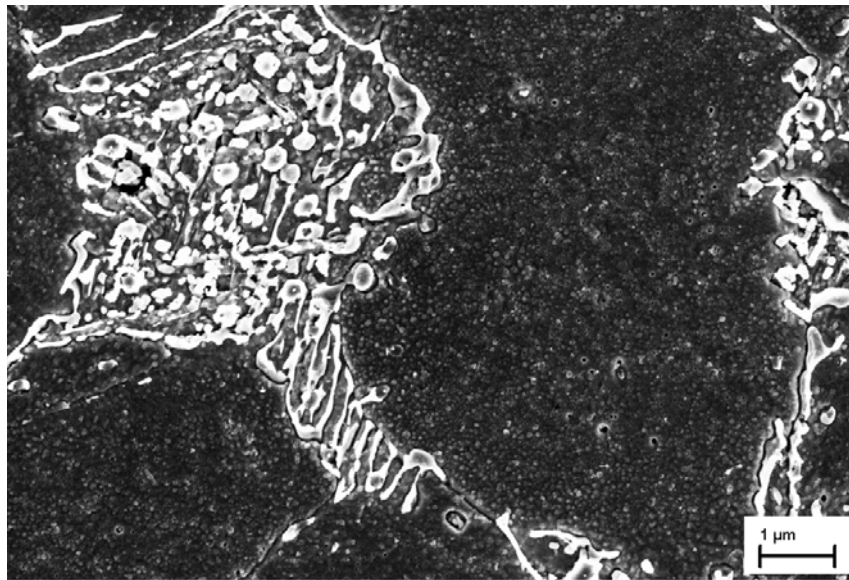


Figure 5. Scanning electron micrograph showing phases present in material which underwent multiple passes of FSP at a much finer scale than the as-cast material.

THIS PAGE INTENTIONALLY LEFT BLANK

III. EXPERIMENTAL PROCEDURE

A. OVERVIEW

This research focuses on comparing the microstructural characteristics of nickel aluminum bronze that has undergone a single pass of FSP to that which has having undergone multiple FSP passes. This was accomplished using optical microscopy and scanning electron microscopy. Additionally, volume fraction determinations and estimated peak temperature calculations were conducted in order to help explain the microscopic results.

B. MATERIAL PROCESSING

Nickel aluminum bronze plates were processed using FSP by Rockwell Scientific Corporation (now Teledyne Scientific Company) using several different RPM and IPM combinations. A step-spiral Densimet® tool with a shoulder diameter of 12.7 mm was used for this processing. Densimet® is an tungsten–iron powder metallurgy material with elevated temperature strength and erosion resistance when used for FSP of nickel aluminum bronzes. From these plates, several samples were cut using a computer controlled Charmilles Andrew EF630 electric discharge machine (EDM) and a consumable brass cutting wire with a nominal diameter of 0.30 mm. Of these samples cut, four were chosen that were sectioned so that the transverse plane (normal to the direction of tool travel) would be visible for analysis.



Figure 6. Example of a rectangular spiral pattern used for FSP of multiple pass plates.

The first sample came from a plate that was processed with a single FSP pass using a tool rotational speed of 800 RPM and a tool traversing rate of 4 IPM. This created a SZ that was 2.3 cm across and 1.2 cm deep. The second sample came from a plate that was processed with multiple FSP passes using the same RPM/IPM combination. This was done in a rectangular spiral pattern (Figure 6) by working from the inside to the outside of the plate and keeping the advancing side of the tool to the outside of the plate. A step over distance of 4.5 mm was maintained between successive passes. The final area processed was 9.8 cm across and 22.5 cm long. The SZ examined in this sample was 5.5 cm long (due to the location of cutting of the sample) and 1.2 cm deep. The third sample came from a plate that was processed with a single FSP pass using a tool rotational speed of 1200 RPM and a tool traversing rate of 2 IPM. This created a SZ that was 2.6 cm across and 1.2 cm deep. The fourth sample came from a plate that was processed with multiple FSP passes using a tool rotational speed of 1200 RPM and a tool traversing rate of 2 IPM. This was, again, done in a rectangular spiral pattern by working from the inside to the outside of the plate and keeping the advancing side of the tool to the outside of the plate. A step over distance of 4.5 mm was maintained between consecutive passes. The final area processed was 9.8 cm across and 22.5 cm long. The SZ examined in this sample was 2.9 cm long (due to the location of cutting of the sample) and 1.2 cm deep. Composition data for the samples of this investigation are as shown in Table 2.

Element	Cu	Al	Ni	Fe	Mn	Si	Pb
800/4	81.0	9.31	4.58	3.51	1.44	0.05	<0.005
1200/2	81.3	9.17	4.46	3.68	1.24	0.06	<0.005

Table 2. Composition data (wt%). From [15].

C. MICROSTRUCTURE ANALYSIS

1. Optical Microscopy

a. *Sample Preparation*

Sample preparation was conducted in several phases including grinding, polishing, and etching. The first step was to grind the surface using a Buehler ECOMET 4 Variable Speed Grinder-Polisher. This was done using a succession of fine grit SiC sandpapers, 400 grit, 1200 grit, 2400 grit, then 4000 grit, with an abundance of water, for about 4 minutes per sandpaper grit at 140 RPM. Upon completion of each step of grinding, the sample was rinsed with copious amounts of water.

Second, using a Buehler ECOMET 3 Variable Speed Grinder-Polisher, samples were polished to a mirror finish. This was accomplished by first using 3 μ Buehler MetaDi Monocrystalline Diamond Suspension (water based) for 15 minutes at 200 RPM. Then, further polishing was done using 1 μ Buehler MetaDi Monocrystalline Diamond Suspension (water based) for 15 minutes at 200 RPM. The final polishing was accomplished using Buehler Mastermet 0.05 μ Colloidal Silica Polishing Suspension at 200 RPM until the samples were completely scratch-free with a mirror finish. Between each step of polishing, samples were rinsed with generous amounts of water, and upon completion of polishing the samples were drenched in methanol and dried with a hot air gun.

The final step in sample preparation was etching of the surface for view in the optical microscope. First, a solution was made using 40 mL of water, 40 mL of ammonium hydroxide, and 2 mL of hydrogen peroxide. A second solution was then

made using 60 mL of water, 30 mL of phosphoric acid, and 10 mL of hydrogen peroxide. The samples were immersed in the first solution for 1–2 seconds and then immediately removed and rinsed with copious amounts of water. Then, the samples were submerged in the second solution for 1–2 seconds and immediately removed and rinsed with water. Finally, the samples were again covered in methanol and dried with a hot air gun to remove all moisture and facilitate optical microscope viewing. All four samples were prepared in this manner.

b. Optical Microscopy Procedure

Optical microscopy was conducted on all four samples. This was accomplished using the Nikon Epiphot 200 optical microscope equipped with a digital imaging system. First, montages were created of all four samples showing the transverse section of the stir zone using a low magnification. This was completed by taking a series of micrographs at a 2.5x magnification covering the entire area of the SZ, HAZ, TMAZ, and some as-cast material in the region of the processed area.

Then, three optical microscopy surveys were prepared to compare the single pass sample and the multiple pass sample having undergone FSP using a tool rotational speed of 800 RPM and a tool traversing rate of 4 IPM. The first survey compared four microstructures at 50x magnification. The four points compared were at equivalent locations 2.5 mm down from the surface in the as-cast material, in the HAZ on the advancing side, 2 mm into the SZ from the SZ boundary on the advancing side, and 4 mm into the SZ from this boundary, as seen in Figure 7a. The second survey compared the progression of the microstructural modification across both samples at a depth of 2.5 mm from the surface at 50x magnification. This survey covered the as-cast material, HAZ on the advancing side, advancing side, mid section of the stir zone, and the retreating side and retreating side HAZ for the single pass, and the multi-processed region for the multiple pass sample, as seen in Figure 7b. The third survey compared a grid of 42 points at corresponding locations in the two samples. The grid was laid out with three rows, each with 14 points (14 columns). The upper row was located at 0.5 mm below the sample's surface, the middle row was located at 5.3 mm below the sample's surface, and

the lower row was located at 9.0 mm below the sample's surface. The starting point for each grid row was located at equivalent locations in the as-cast material for both samples, with the subsequent grid points spaced 2 mm apart. The grid for this survey can be seen in Figure 7c.

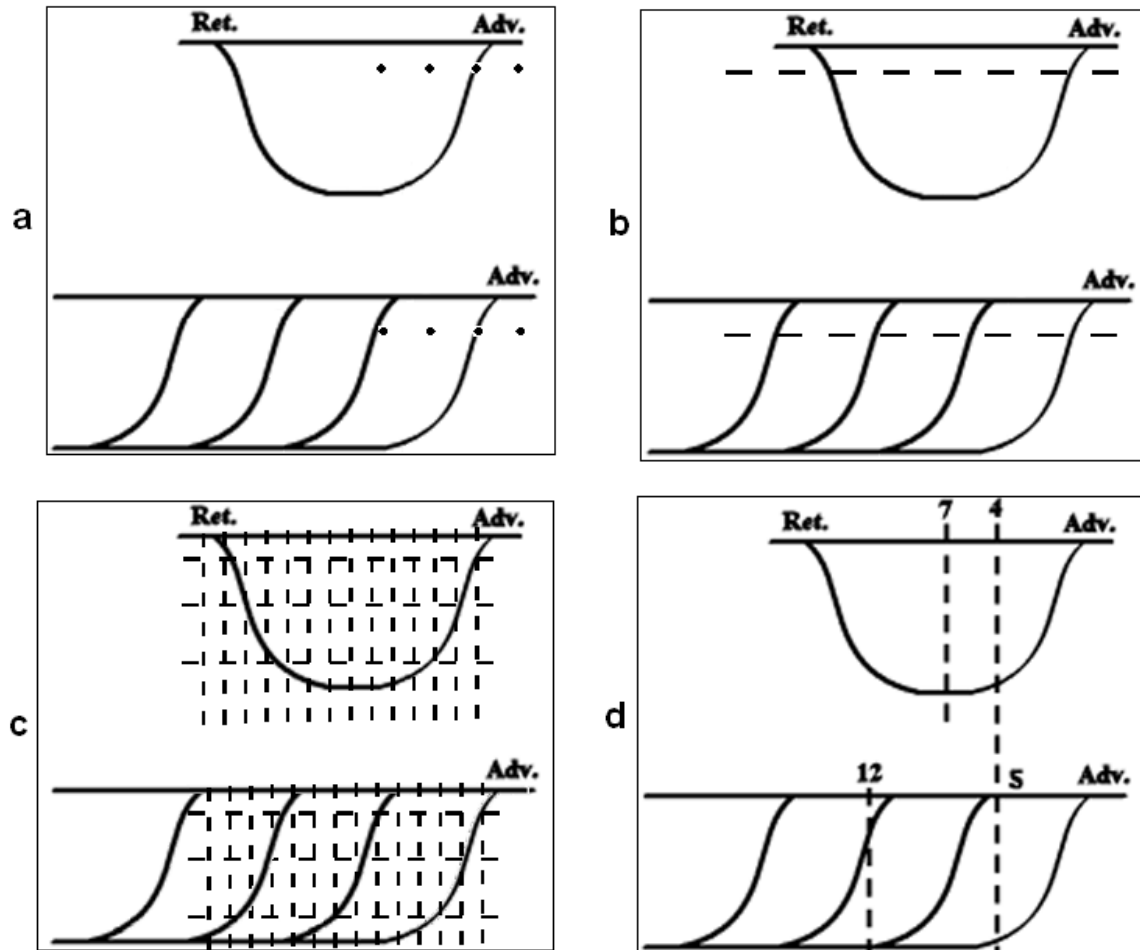


Figure 7. Schematic showing location in SZ of optical microscopy surveys: a) locations for first survey; b) locations for second survey; c) locations for third survey and area used for optical montages; d) column locations for use in volume fraction and estimated peak temperature determinations.

2. Scanning Electron Microscope

a. Sample Preparation

All four samples were also examined by Scanning Electron Microscopy. To ensure electrical continuity, each sample was prepared by applying a thick coat of PELCO Colloidal Silver #1603-4 to the back side of the sample and attaching it to a specimen holder. Finally, the samples were placed in a vacuum chamber for approximately an hour in order to ensure adhesion and thorough drying.

b. Scanning Electron Microscopy Procedure

Scanning Electron Microscopy (SEM) was accomplished using the Zeiss Neon 40 SmartSEM V05.03 Field Emission Scanning Electron Microscope. First, from the samples having undergone FSP at 800 RPM and 4 IPM, using column numbers referenced from the third optical survey grid, two columns were chosen for volume fraction measurements. Column 4 in the single pass sample and column 5 in the multiple pass sample were chosen due to their corresponding locations relative to the advancing side of the SZ. The column numbers are not identical due to variances in the SZ shapes. Furthermore, column 5 (in the multiple pass sample) is located in a region where only the outermost, final pass has processed the material. In the single pass sample, column 7 was chosen as a location at the approximate center of the SZ. Finally, column 12 in the multiple pass sample was chosen as a location which had undergone multiple, overlapping passes. The column locations mentioned are seen in Figure 7d.

Once the column locations for volume fraction determinations were chosen, SEM micrographs were taken using secondary electron or backscatter imaging modes. For each column, the first micrograph location was taken 0.5 mm below the surface of the sample and subsequent locations were at 1.0 mm spacing down through the SZ. At each location, four micrographs were taken at a spacing of 0.2 mm horizontally.

For the two samples that had undergone FSP at 1200 RPM and 2 IPM, micrographs were taken at locations corresponding to those in the samples having undergone FSP at 800 RPM and 4 IPM. Thus, these locations included, in the single pass

sample, the advancing side and the center on the SZ, and for the sample having undergone multiple passes, the outermost, final pass and a region having undergone multiple passes. The first micrograph was, again, taken 0.5 mm below the sample's surface with subsequent micrograph locations taken down through the SZ in 1 mm intervals. At each location, again, four micrographs were taken at a spacing of 0.2 mm horizontally.

Additionally, micrographs were taken at 0.2 mm below the surface, in the middle of the SZ, in the SZ just above the SZ-HAZ interface, in the HAZ, and in the base metal for all four samples for microstructural comparisons and validation of estimated peak temperature determinations. Montages were also created using SEM micrographs for column 7 on the single pass samples and column 12 on the samples which underwent multiple passes.

D. VOLUME FRACTION DETERMINATION

From the micrographs taken using the SEM, the volume fraction of the α phase was determined for the locations along the two columns in each sample. First, a grid of 216 points (12 x 18) was overlain on each micrograph as seen in Figure 8. Then, the points which corresponded to a location in the α phase (the dark etching constituent), were counted. This sum was divided by the total number of points (216) yielding the volume fraction of α phase. This was repeated over 400 times. Then the average of the four micrographs at each location was taken and plotted versus the depth in the SZ. To determine the estimated peak temperature at each location, the volume fraction of β transformation products was needed. This fraction was simply equivalent to one minus the volume fraction of the α phase ($V_{\beta} = 1 - V_{\alpha}$), where V_{α} and V_{β} represent the volume fractions of the α and β phases, respectively.

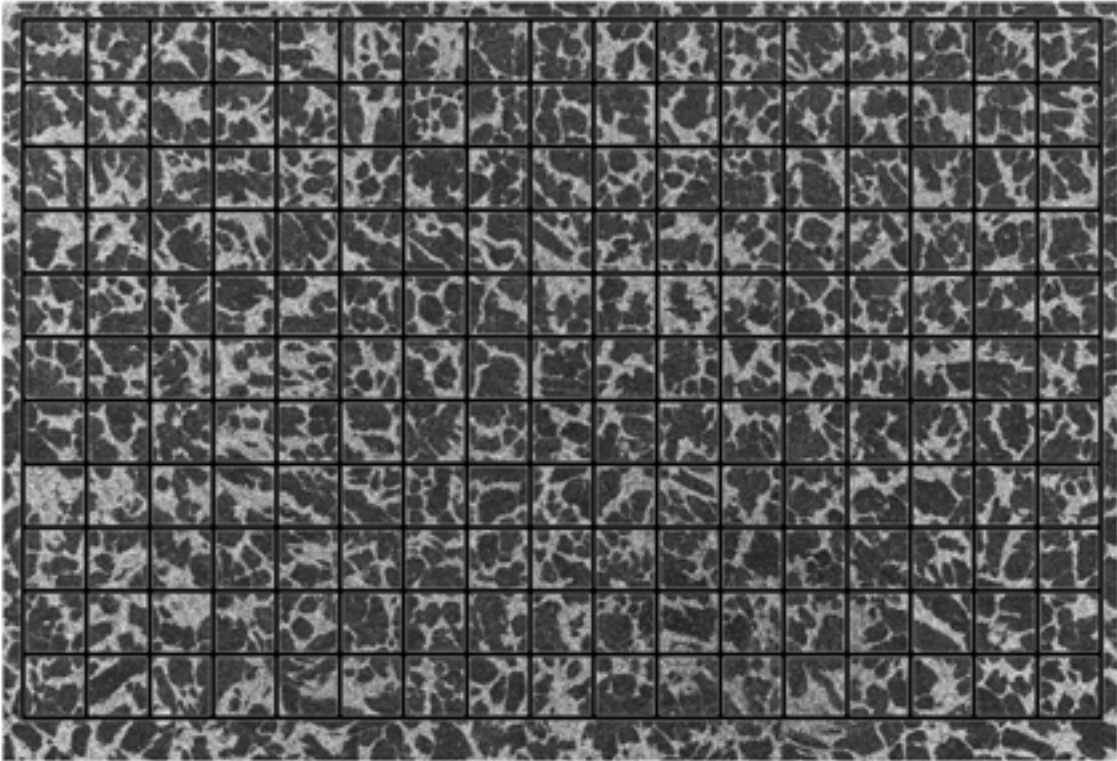


Figure 8. Scanning electron micrograph of an area which underwent FSP with an overlaid grid used for volume fraction determinations.

E. ESTIMATED PEAK TEMPERATURE DETERMINATION

From the volume fraction of β transformation products (V_{β}), the estimated peak temperature at each location could be calculated. This was accomplished using the equation $T = 244 V_{\beta} + 758$ determined in previous work, with the resultant temperature in degrees Celsius [16]. The estimated peak temperature was also plotted versus the depth in the SZ, such plots will be shown in the following chapter.

IV. RESULTS

A. OVERVIEW

Four samples were studied which had undergone FSP with two different processing conditions, a rotational rate of 800 RPM and a tool traversing rate of 4 IPM or 1200 RPM and 2 IPM. For each condition, one sample had received a single pass of FSP and the other sample was processed with multiple passes in a rectangular spiral pattern. Results from optical microscopic analysis, volume fraction determinations, peak temperature determinations, and subsequent microscopic study with the SEM are presented in this chapter.

B. OPTICAL MICROSCOPY

These four samples were initially studied using optical microscopy. The first sample had experienced a single pass of FSP at a rotational speed of 800 RPM and a traversing rate of 4 IPM and can be seen in Figure 9a. The second sample experienced multiple FSP passes at 800 RPM and 4 IPM and can be seen in Figure 9b. The third sample was processed using a single FSP pass at a rotational speed of 1200 RPM and a traversing rate of 2 IPM and can be seen in Figure 10a. The fourth sample was processed with multiple passes of FSP at 1200 RPM and 2 IPM and can be seen in Figure 10b. In Figures 9 and 10, the advancing side can be seen on the right and the retreating side is on the left. For Figures 9b and 10b, the outermost, final pass material is on the right side.

From the optical montages in Figures 9 and 10, it can be seen that a relatively homogeneous and refined microstructure has been achieved on the macro scale. However, in both of the single pass samples inhomogeneity is apparent on the retreating side of the SZ as can be seen by an indistinct boundary between the TMAZ and the SZ. These inhomogeneities are removed by the application of successive passes on the retreating side. Also seen in the single pass and the multiple pass samples are 'onion ring' flow patterns. Furthermore, in the multiple pass samples several bands can be seen which reflects successive passes in the SZ. These bands are only visible, though, at low

magnification and consist of patterns of varying refinement in the microstructure. These inhomogeneities have also all been noted in previous work [15, 17]. From the optical montages other possible differences in microstructure are unclear between the single and multiple pass samples, and the distinction between the phases is impossible to differentiate due to the refined microstructure.

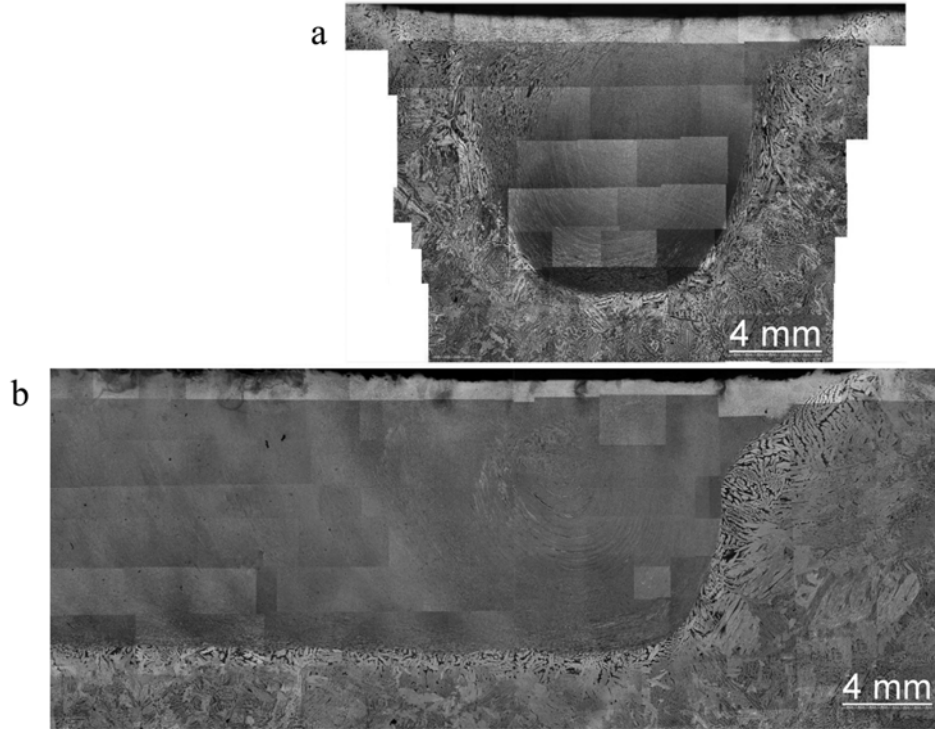


Figure 9. Optical montages of micrographs from: a) Sample which underwent a single pass of FSP at 800/4; b) Sample which underwent multiple passes of FSP at 800/4.

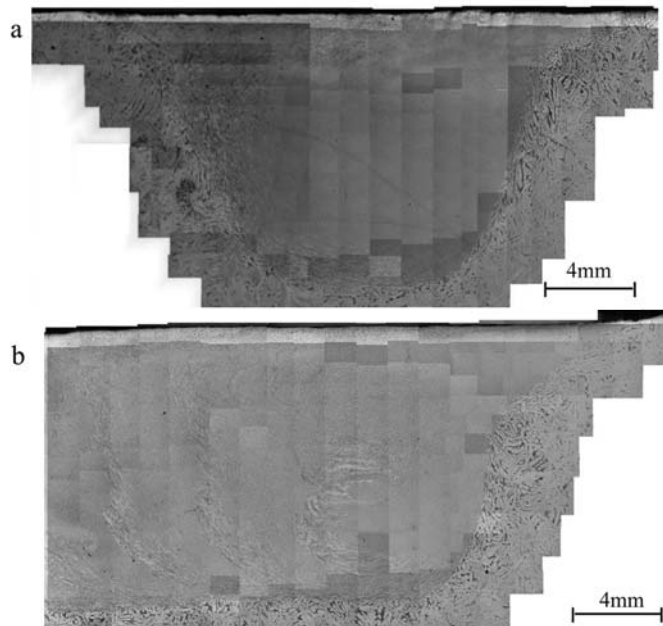


Figure 10. Optical montage of micrographs from: a) Sample which underwent a single pass of FSP at 1200/2; b) Sample which underwent multiple passes of FSP at 1200/2.

Optical surveys were also completed comparing approximate locations in the samples having undergone FSP at a rotational speed of 800 RPM and a tool traversing rate of 4 IPM. From these surveys it was seen that the approximate volume fraction of β transformation products appeared to be smaller in the multiple pass sample than the single pass sample, as is evident by less dark etching in Figures 11c and 11d than in Figures 11a and 11b. Additionally, the size of the α grains were noticeably coarser in the multiple pass sample than the single pass sample, as is evident by Figures 12a–d. In comparing Figures 11 through 13, it can also be seen that the grain size is coarser at locations higher in the SZ and the grain become finer with depth. This result is consistent with previous work [18]. Also evident in comparing micrographs from the multiple pass sample is that the microstructure is finer in the multiple pass region than in the outermost pass region. This can be seen by examining Figures 12c and 12d, where Figure 12d has an apparently finer microstructure than Figure 12c.

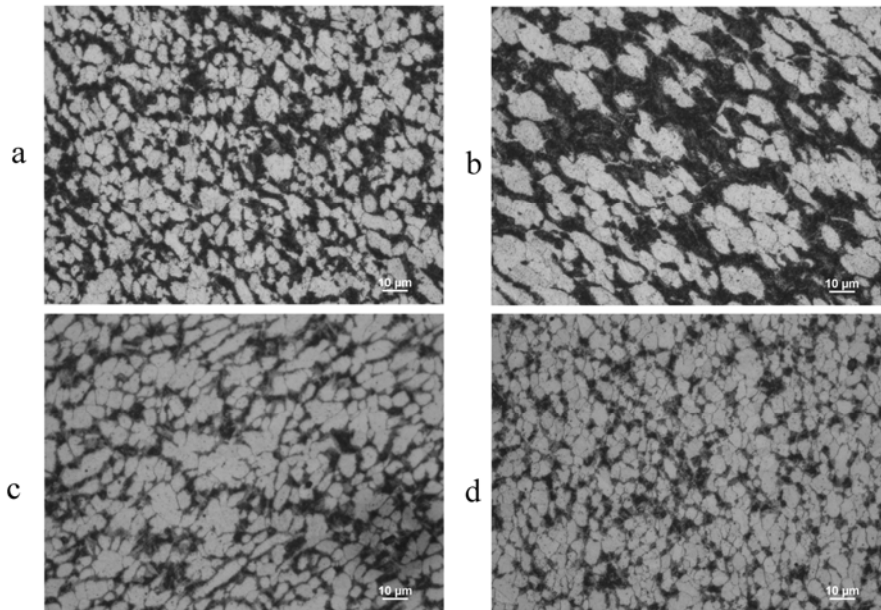


Figure 11. Optical micrographs from 0.5 mm below surface of sample: a) 800/4 single pass column 4; b) 800/4 single pass column 7; c) 800/4 multiple passes column 5; d) 800/4 multiple passes column 12.

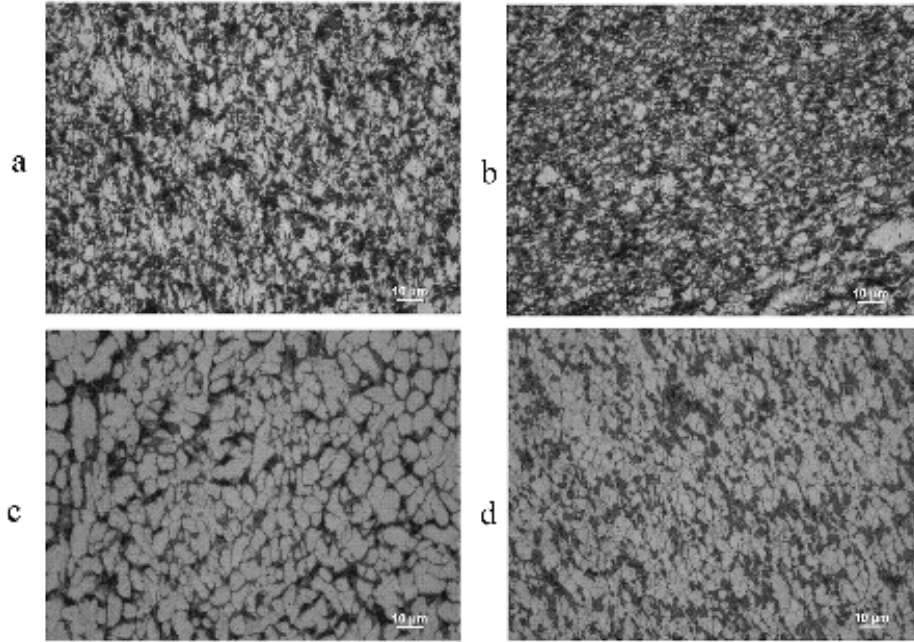


Figure 12. Optical micrographs from 5.3 mm below surface of sample: a) 800/4 single pass column 4; b) 800/4 single pass column 7; c) 800/4 multiple passes column 5; d)800/4 multiple passes column 12.

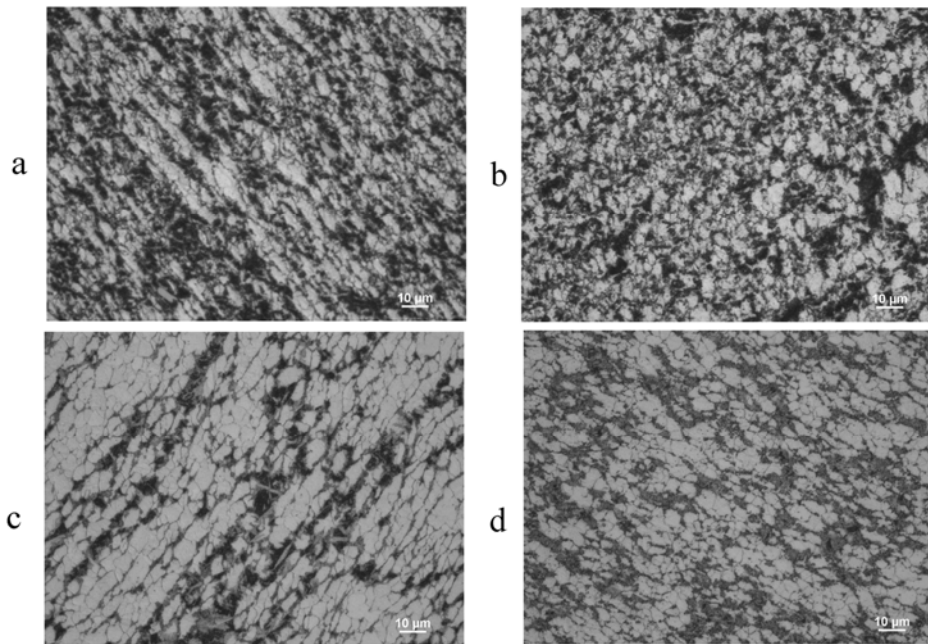


Figure 13. Optical micrographs from 9.0 mm below surface of sample: a) 800/4 single pass column 4; b) 800/4 single pass column 7; c) 800/4 multiple passes column 5; d)800/4 multiple passes column 12.

C. VOLUME FRACTION DETERMINATION

Using the SEM, micrographs were acquired at locations in the SZ along the columns of points corresponding to those used for optical microscopic surveys. These were: on the advancing side of the single pass samples, column 4; the middle of the single pass samples, column 7; the outermost pass in the multiple pass samples, column 5; and a region which underwent multiple passes, column 12. The column locations mentioned can be seen in Figure 7d. For the four samples, the volume fraction of the α phase was calculated as a function of SZ depth for the two pertinent columns per sample. Again, the volume fraction of the α phase was determined by point counting as described under Experimental Procedure.

The volume fraction determinations were based on SEM micrographs as discussed previously. All the images used were taken in the secondary electron imaging mode, which was clearly able to delineate the α phase. From these images it was also clear that the α grains were equiaxed and recrystallized. Additionally, at the magnification used, the fine κ_{iv} phase could be seen. Therefore, the transformed β phase resolved into highly a refined $\alpha + \kappa_{iii}$, as well as κ_{iv} phase.

The volume fraction determination results for the samples which were processed at 800 RPM and 4 IPM are shown in Figure 14 and the results for the samples which were processed at 1200 RPM and 2 IPM are shown in Figure 15. Figure 16 compares two locations in the 800 RPM and 4 IPM multiple pass sample with the same two locations in the 1200 RPM and 2 IPM sample. The micrographs all reflect similar corresponding microstructures, but it is evident that there is more light features seen in Figures 16a and 16b than in Figures 16c and 16d. Also seen from Figure 16 is the homogenization created by using multiple FSP passes. From Figures 14 and 15, it is possible to additionally see that the volume fraction of the α phase does not vary as much for the multiple pass samples when comparison is made to the single pass samples.

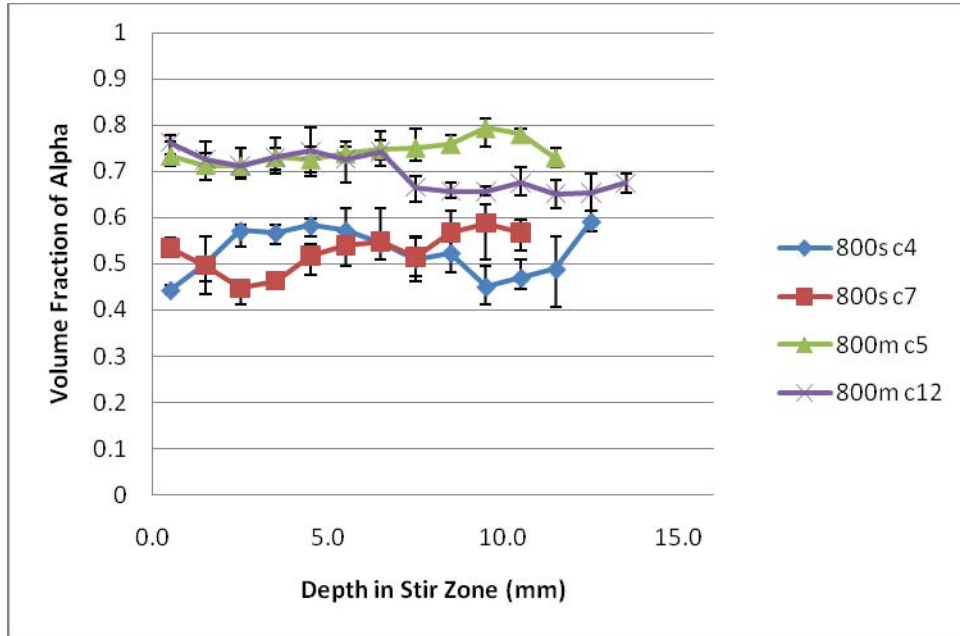


Figure 14. Volume fraction of α phase determinations for the samples having undergone FSP at a rotational speed of 800 RPM and a traversing rate of 4 IPM. In legend 's' signifies single pass sample, 'm' signifies multiple pass sample, and 'c' signifies the approximate column location.

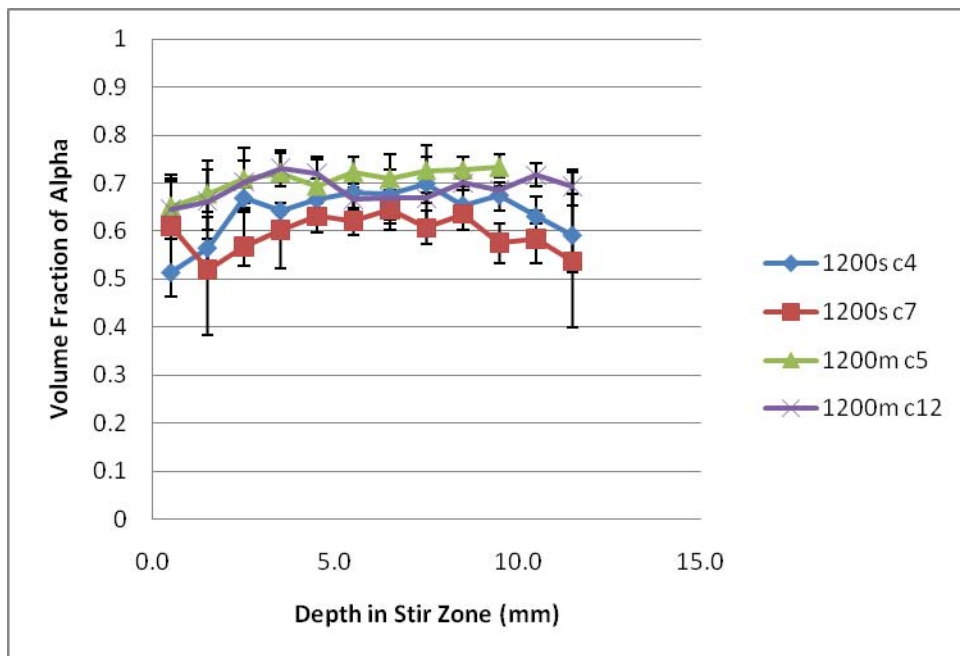


Figure 15. Volume fraction of α phase determinations for the samples having undergone FSP at a rotational speed of 1200 RPM and a traversing rate of 2 IPM. In legend 's' signifies single pass sample, 'm' signifies multiple pass sample, and 'c' signifies the approximate column location.

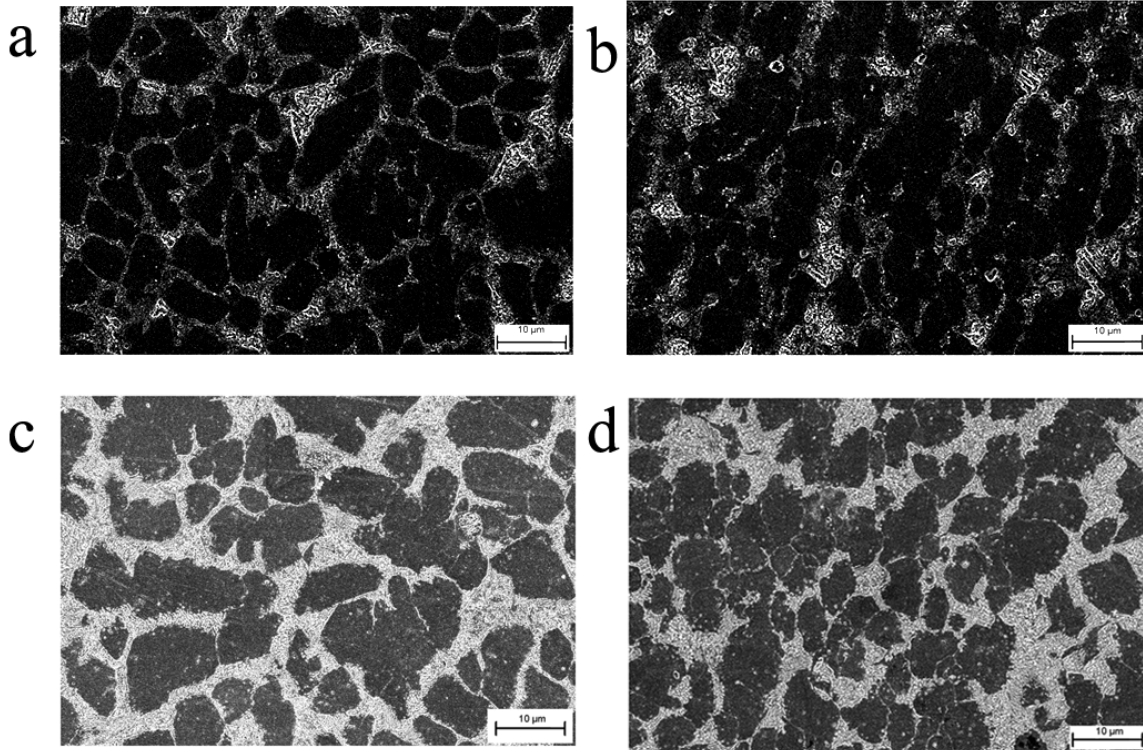


Figure 16. SEM micrographs from multiple pass samples : a) 800/4 column 5; b) 800/4 column 12; c) 1200/2 column 5; d) 1200/2 column 12

D. ESTIMATED PEAK TEMPERATURE DETERMINATION

From the results for the volume fraction of the α phase it was possible to determine the estimated peak temperature at each location in the SZ. First the volume fraction of the α phase needed to be converted to the volume fraction of β transformation products at each location by using the equation $V_{\beta} = 1 - V_{\alpha}$. Then, using the equation $T = 244 V_{\beta} + 758$, determined in [16], the estimated peak temperature (in $^{\circ}\text{C}$) could be determined for each point in the SZ that a volume fraction calculation was taken. The plots for estimated peak temperature versus depth in the SZ are shown in Figures 17 and 18. The single pass temperature curves seen are consistent with previous work [16].

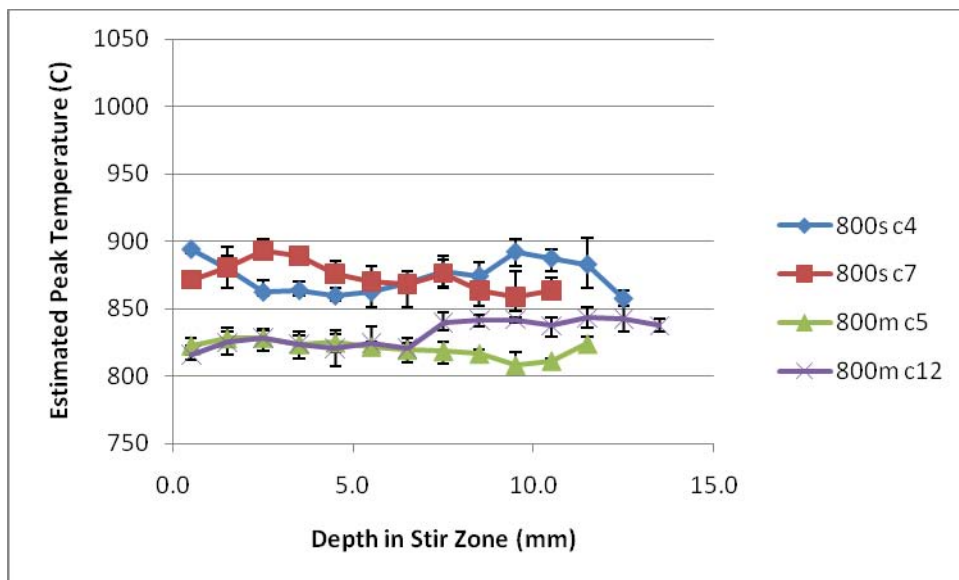


Figure 17. Estimated peak temperature determinations for the samples having undergone FSP at a rotational speed of 800 RPM and a traversing rate of 4 IPM. In legend ‘s’ signifies single pass sample, ‘m’ signifies multiple pass sample, and ‘c’ signifies the approximate column location.

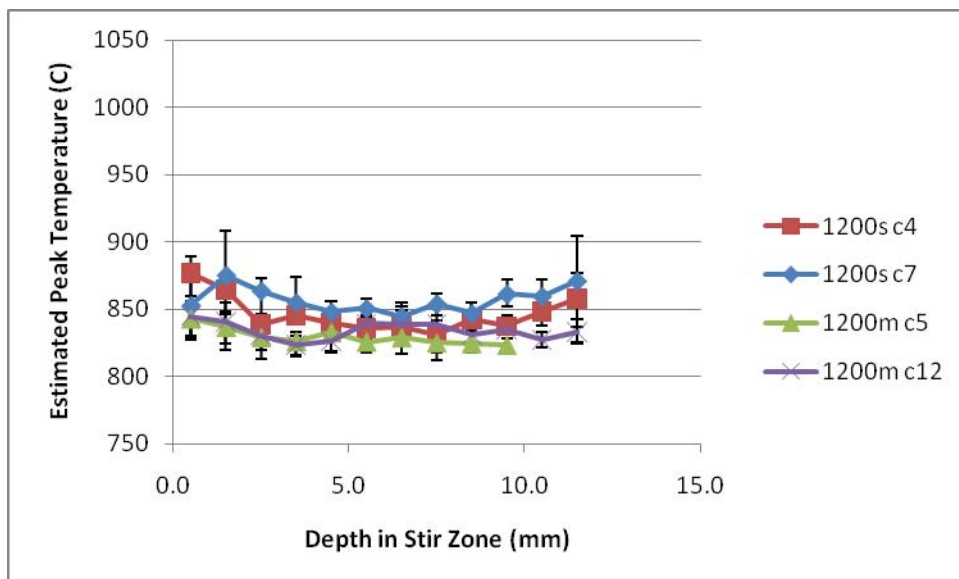


Figure 18. Estimated peak temperature determinations for the samples having undergone FSP at a rotational speed of 1200 RPM and a traversing rate of 2 IPM. In legend ‘s’ signifies single pass sample, ‘m’ signifies multiple pass sample, and ‘c’ signifies the approximate column location

As can be seen in Figures 17 and 18, for the samples which underwent multiple FSP passes, the average estimated temperatures are approximately the same, with a slight increase in temperature seen due to the increased heat input in the 1200 RPM and 2 IPM sample. The average temperature for the sample which was processed at 800 RPM and 4 IPM with multiple passes was 826 °C, while the average temperature for the sample processed at 1200 RPM and 2 IPM with multiple passes was 832 °C. For both sets of processing conditions it can also be seen that the multiple pass sample local temperatures are consistently lower than the single pass local temperatures. For the 800 RPM and 4 IPM single pass sample, the average estimated temperature was 874 °C, while for the sample which was processed at 1200 RPM and 2 IPM had an 852 °C average temperature. The difference in temperature was therefore 48 °C for the 800 RPM and 4 IPM samples and 20 °C for the 1200 RPM and 2 IPM samples.

V. DISCUSSION

Comparison of the as-cast microstructure (Figure 4) to the microstructures produced by FSP (e.g., Figures 11–13 and 16) shows that such processing of nickel aluminum bronze yields a refined, homogeneous microstructure. A single pass of FSP substantially refines and homogenizes microstructure, while multiple passes have been shown to lead to further homogenization. It was also seen that the SZ in samples which underwent a single FSP pass experienced higher temperatures than those in the multiple pass samples. The temperature attained for multiple pass samples showed less apparent dependence on processing conditions and location in the SZ whereas the temperature attained on single pass samples varied more with location and conditions.

Montages created using the SEM are shown in Figures 19–22. These four montages show the homogenous microstructure throughout the SZ. As can be seen, the majority of the SZ in material which underwent FSP consists of fine, equiaxed α phase, the dark constituent, with smaller amounts of β transformation products, the light constituent. The large dark regions seen in Figures 19–21 are dust shadows and should be ignored. In the montages of the two single pass samples, Figures 19 and 21, it can be seen that the inhomogeneous features at the top and bottom of the SZ are more extensive than in the two montages of the multiple pass samples, Figure 20 and 22.

The inhomogeneous region at the top of the SZ consists of a lamellar arrangement of dark α phase and a mixture of martensite or bainite in which Widmanstätten α phase also formed. These features likely reflect the effect of the tool shoulder as it pulls base metal into the upper region of the SZ in the final stages of deformation. This creates deformed and elongated grains in the direction of the shear stress which have experienced less deformation. Previous work has shown that in this region, the yield strength more than doubles and the ultimate tensile strength increase 89% for a single pass sample, in comparison to the as-cast material [19]. Highly magnified micrographs of this near tool region can be seen in Figure 23. In Figures 23c and 23d, it can be seen that in the

multiple pass sample, at a depth of 0.2 mm the grains are becoming less elongated than Figures 23a and 23b, and that the homogeneous microstructure starts higher in the SZ for the multiple pass sample.

The inhomogeneity at the bottom of the SZ corresponds to a region below the depth of the tool pin. The region undergoes less stirring action by the pin due to its location and therefore less plastic deformation. The grains in this region are also elongated, though they are less elongated than at the top of the SZ.

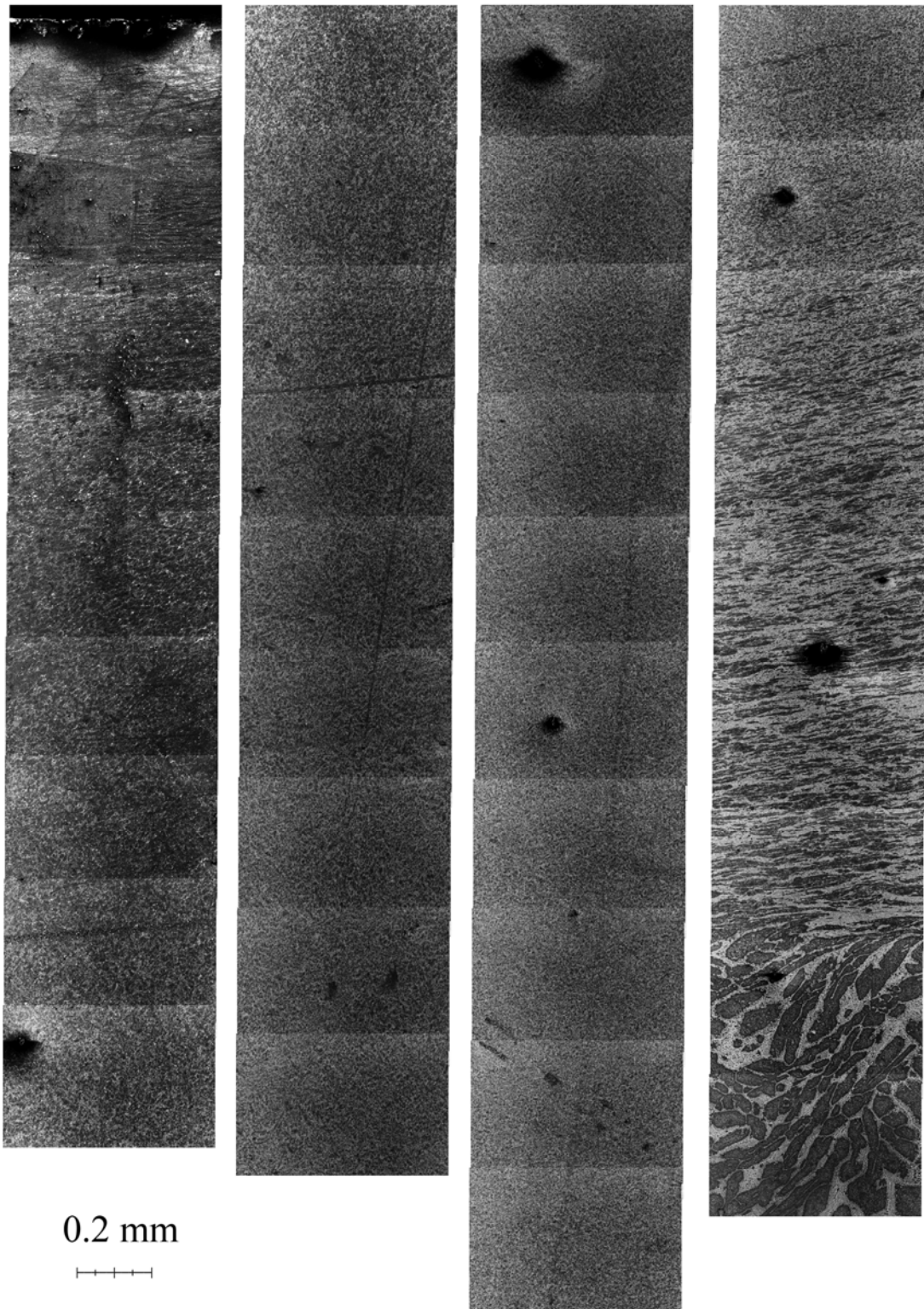


Figure 19. SEM montage of micrographs for 800 RPM and 4 IPM, single FSP pass sample, column 7.

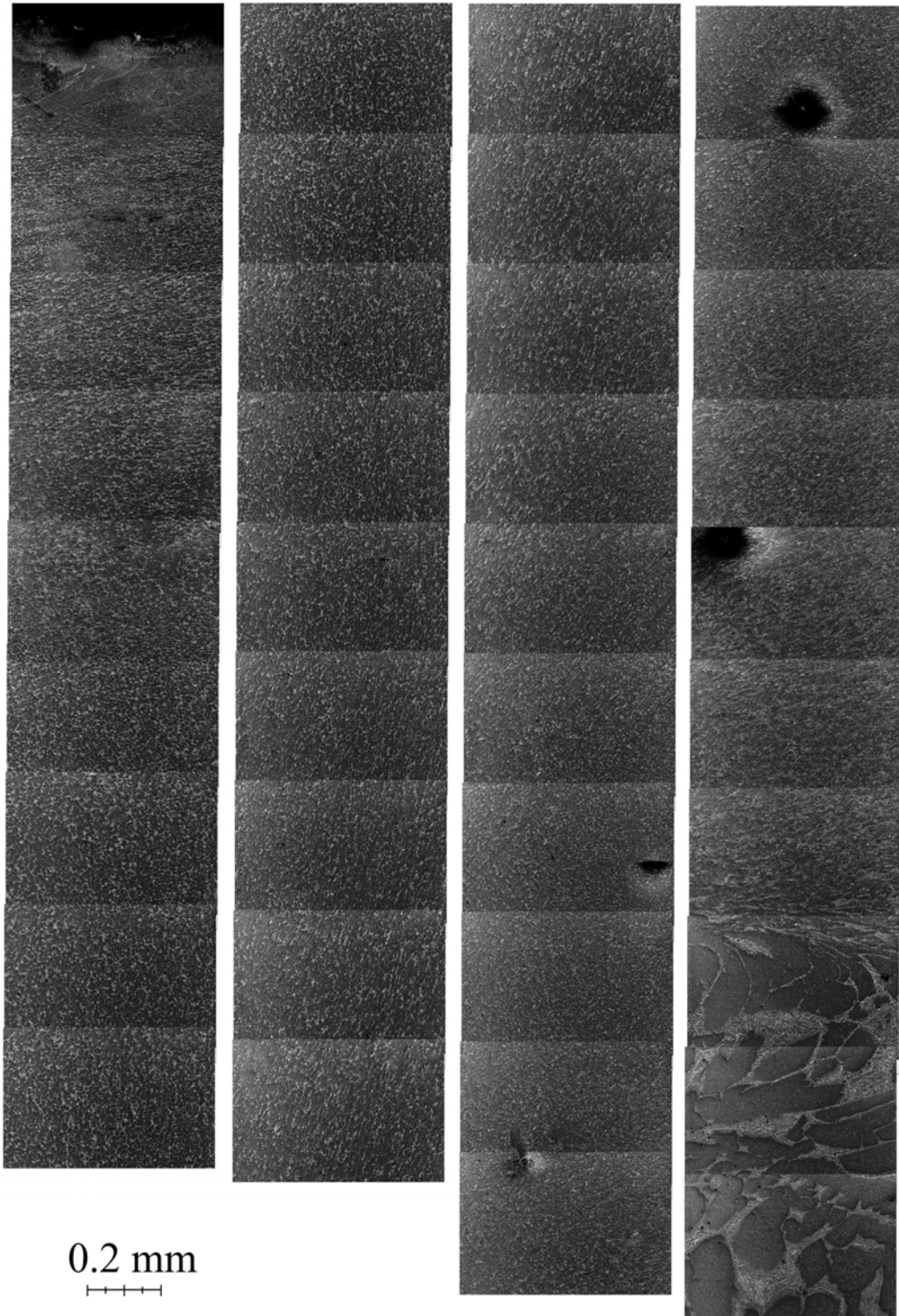


Figure 20. SEM montage of micrographs for 800 RPM and 4 IPM, sample processed with multiple FSP passes, column 12.

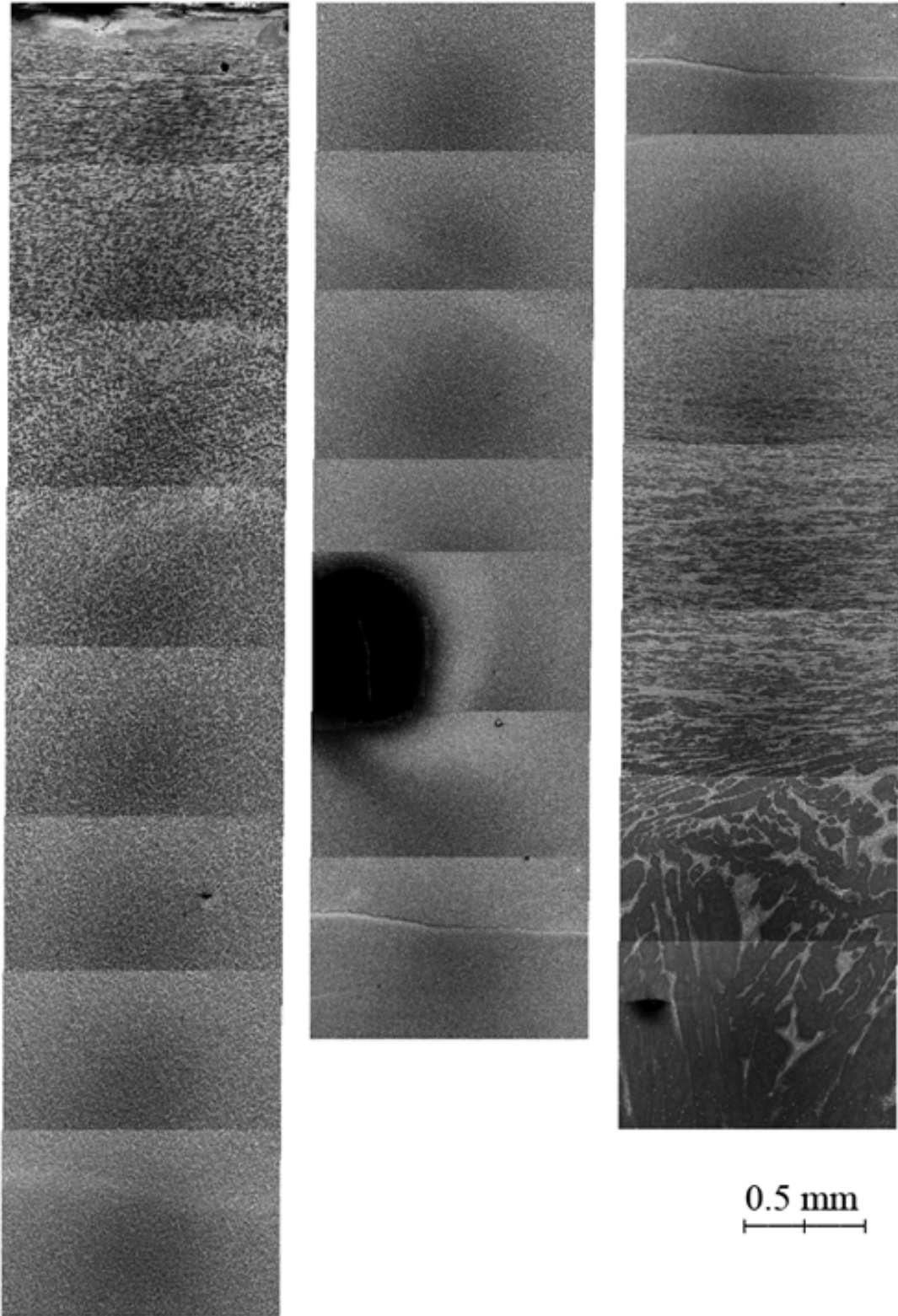


Figure 21. SEM montage of micrographs for 1200 RPM and 2 IPM, single FSP pass sample, column 7

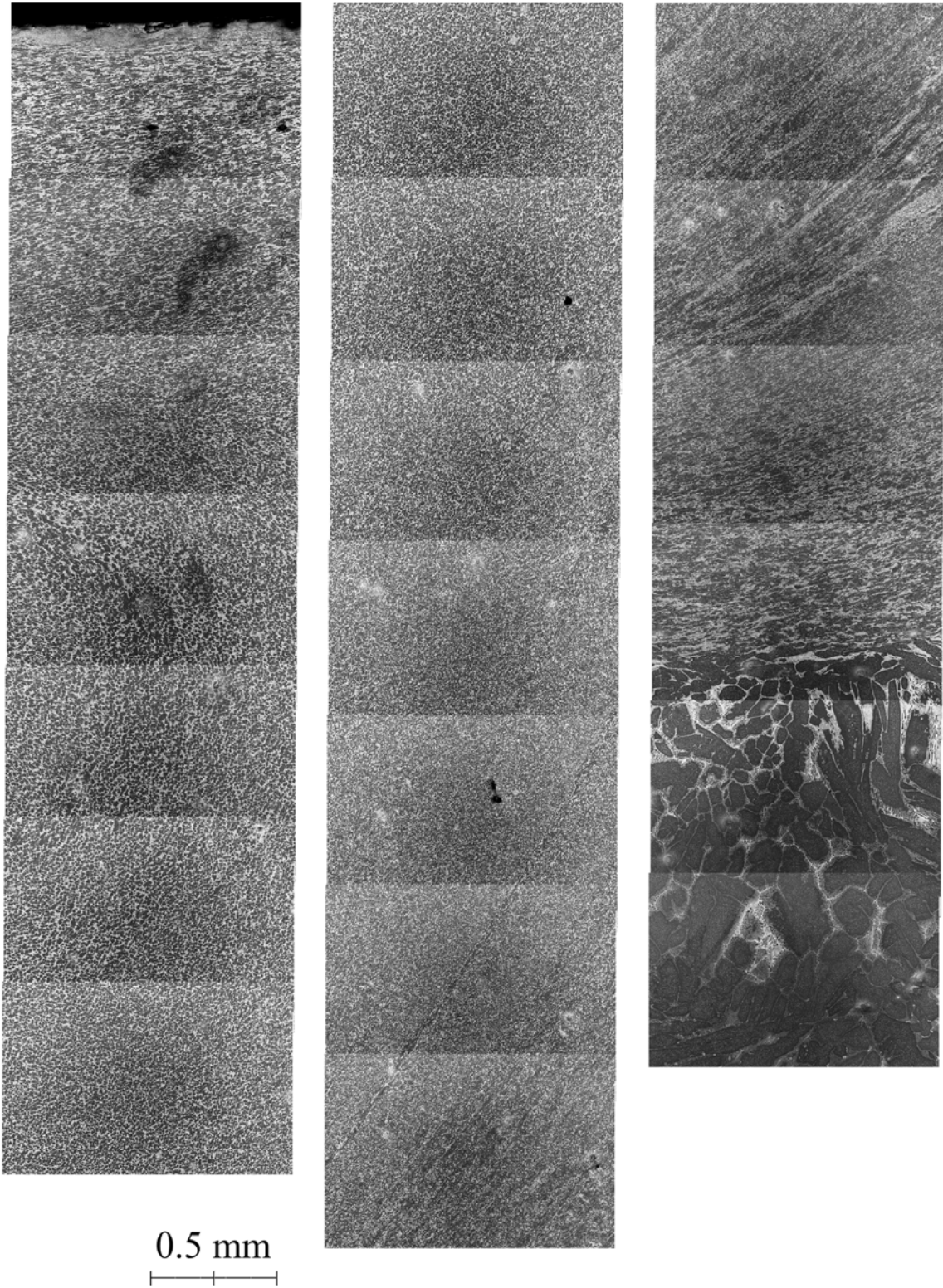


Figure 22. SEM montage of micrographs for 1200 RPM and 2 IPM, sample processed with multiple FSP passes, column 12.

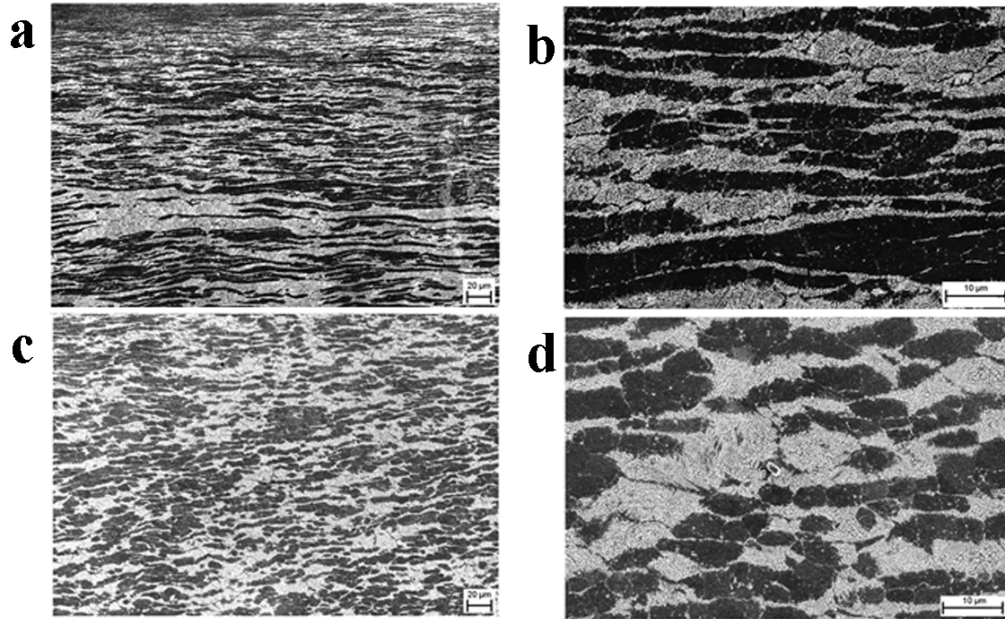


Figure 23. SEM micrographs for 1200 RPM and 2 IPM, 0.2 mm below sample surface: a) Single pass, Column 7, 300x magnification; b) Single pass, Column 7, 1500x magnification; c) Multiple pass, Column 12, 300x magnification; d) Multiple pass, Column 12, 1500x magnification.

Williams conducted mechanical testing on miniature tensile samples obtained from a plate that had been subject to a single FSP pass using a rotational speed of 1000 RPM and traversing rate of 4 IPM [20]. Tensile samples were cut using the wire electric discharge machine (EDM) from the retreating side, the center, and the advancing side at various depths in the SZ. Results from stress versus strain testing as a function of location in the SZ were compiled for the ultimate tensile strength and percent elongation as shown in Figure 24. These results show that a single FSP pass results in the near doubling of the ultimate tensile strength while the percent elongation was also increased by an average of about 6%.

Also seen from Williams work is that for a single pass sample, the material properties depended greatly on the location in the SZ. Both the ultimate tensile strength and the percent elongation have large variances depending on SZ location. In Figures 17 and 18, it was seen that the estimated peak temperature also varied for the single pass samples depending on the location in the SZ. Williams work demonstrates that the best properties correspond to the center of the SZ. From the montages in Figures 19 and 21, it

can be seen that a region of fine, equiaxed α phase in a highly homogeneous distribution of constituents exists when compared to the as-cast material. The grain refinement would account for the increased strength and the improved homogenization would yield the increased ductility seen the Williams work.

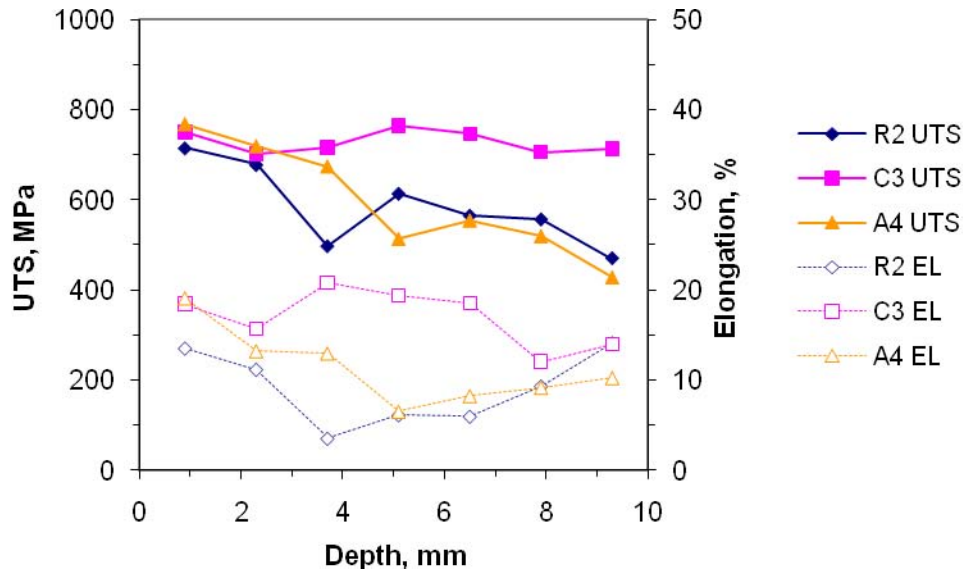


Figure 24. Ultimate tensile strength and elongation data for sample which underwent a single pass of FSP at 1000 RPM and 4 IPM with a 13 mm tool diameter. From [12].

Miniature tensile samples were machined by wire EDM from the same multiple pass plates as the samples in this research for mechanical testing by Rosemark [15]. The samples were cut along the depth of the SZ for a region containing multiple passes for both the 800 RPM and 4 IPM and 1200 RPM and 2 IPM processing combinations. Results from stress versus strain curves were compiled, and selected results are shown in Figure 25. From this research it can be seen that in samples which experienced multiple FSP passes the yield strength and ultimate tensile strength approximately doubled compared to the as-cast condition and the percent elongation was increased to 20–30 % elongation to fracture on average, more than double the percent elongation shown by the single pass results of Williams.

From the montages in Figures 20 and 22, it was seen that the microstructure in the multiple pass samples was more homogeneous throughout the entirety of the SZ. This

increased homogeneity can explain the increase in the ductility seen compared to the single pass material. From Rosemark's work it can also be seen that the increased strength had little dependence on the processing conditions (RPM and IPM). It was seen in Figure 17 and 18 that the estimated peak temperature additionally had little dependence on processing conditions for multiple pass samples. Lastly, also noted in Rosemark's work is a region of lower ductility in the vicinity of the first pass of a sample which underwent multiple passes. This can be explained by a higher temperature achieved in the first pass since it essentially is a single FSP pass.

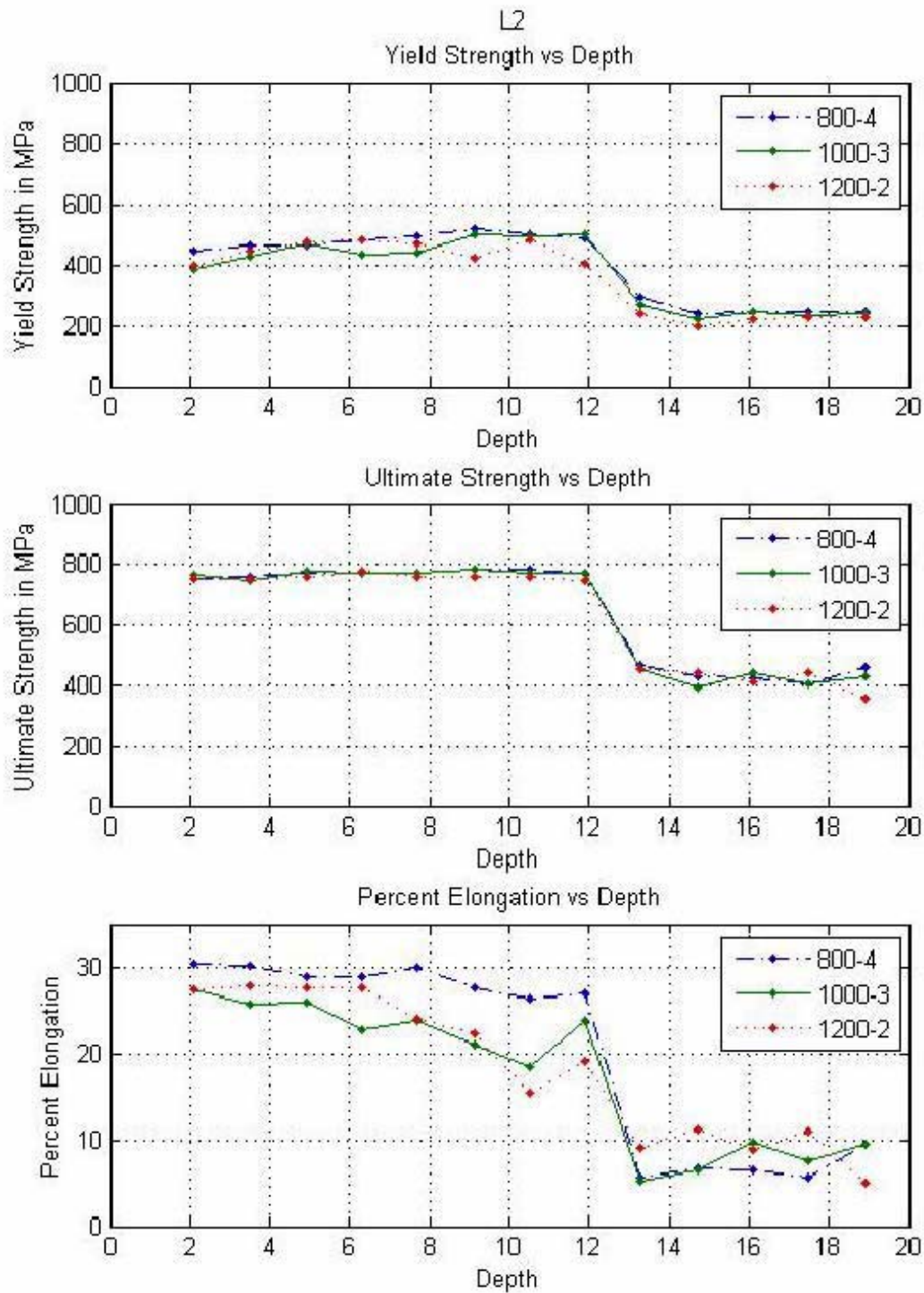


Figure 25. Mechanical property data for multiple pass region in material which underwent FSP with multiple passes. RPM-IPM combinations given in legends. From [10].

In the samples that experienced multiple FSP passes it was seen that the estimated local peak temperatures were lower than those seen in the single pass samples. In the single pass samples the average estimated peak temperature was 863 °C, and in the multiple pass samples the average was 830 °C. From these average temperatures it can be seen that during FSP, the transformations which occurred upon cooling followed either the far right path or the path second from the right in Figure 3. The microstructures seen in scanning electron microscopy as seen in Figure 5 are consistent with the majority of the multiple pass SZ and are again the microstructures predicted from the far right path in Figure 3.

In addition to lowering the estimated peak temperatures, and further homogenization of the SZ, multiple FSP passes lead to an extended dwell at elevated temperatures was created by the addition of successive passes. This dwell at elevated temperature preheats some of the material that was seen in the subsequent passes. It has been determined in previous work that preheating lowers cooling rates and additionally increases dwell times, though it has little effect on the actual peak temperatures [16].

The more homogeneous appearance of microstructure in the multiple pass material reflects increased strain throughout the resulting SZ. Microstructure based estimates of local strain as well as temperature are needed to assess the complete thermo-mechanical history of the SZ and thereby establish tool and processing conditions that will assure high and uniform properties throughout the volume of propeller material subject to this process.

In the application of surface processing of propellers, the variable thicknesses present yield variable cooling rates across the propeller. This, along with the fact that any heat input can produce distortion, has led researchers to envision the use of temperature sensing equipment to control the microstructure created by FSP. Either optical pyrometers or embedded thermocouples in the tool could be used to sense the tool shoulder temperature and then control the processing conditions based on this temperature. It is of importance to note, though, that, as can be seen from Figures 16 and 17, the temperature does not remain constant from the initial pass to the end of processing. The initial pass is essentially material which has undergone a single FSP

pass and therefore attains a higher temperature than subsequent passes that process some new material and some prior processed material.

In the samples which underwent FSP with multiple passes, each subsequent pass processed material which had not already seen the effects of the tool and material which had been processed at least once previously. The extent of the material which was prior processed and how many times that material was processed is not known due to the complex movement of the material in the SZ around the tool. This complex movement also creates an intricate thermo-mechanical history, which cannot currently be predicted.

VI. CONCLUSIONS

1. The temperature profile determined for the sample having undergone FSP at a rotational rate of 800 RPM and a traversing rate of 4 IPM was similar to previous work.

2. The microstructure based, estimated local peak temperatures are lower in the sample which had undergone FSP with multiple passes for 800 RPM and 4 IPM in both the area of the final pass and the region encountered by multiple passes. The average local peak temperature was lowered from approximately 874°C to 826°C (48°C). This decreased temperature led to an increased volume fraction of α phase in the SZ.

3. The temperature profile determined for the sample having undergone FSP at 1200 RPM and 2 IPM was also similar to previous work.

4. The microstructural based, estimated local peak temperatures are, again, lower in the sample which had undergone FSP with multiple passes for 1200 RPM and 2 IPM in both the area of the final pass and the region encountered by multiple passes. The average local peak temperature was lowered from approximately 852°C to 832°C (20°C). This decreased temperature also led to an increased volume fraction of α phase in the SZ.

5. Both the size and morphology of the microstructure in the material having undergone FSP with multiple passes is more homogeneous, though it is also somewhat coarser. The added strain from the multiple passes accounts for the homogeneity, while the increased dwell time at high temperature accounts for the larger grain size.

6. Improved models of microstructure evolution during FSP to account for the effect of strain as well as temperature are needed to enable a complete assessment of the effects of this processing on properties of components.

THIS PAGE INTENTIONALLY LEFT BLANK

VII. RECOMMENDATIONS FOR FUTURE WORK

1. Investigate the effects on the strain and strain rate due to multiple FSP passes.
2. Investigate the effects of changing either the rotational speed or the traversing rate on the estimated peak temperature.
3. Investigate the correlation between externally sensed temperature data and the microstructure in the SZ and the subsequent material properties.
4. Develop models for strain as well as temperature effects on microstructure evolution during FSP of nickel aluminum bronze.

THIS PAGE INTENTIONALLY LEFT BLANK

LIST OF REFERENCES

- [1] P. Wenschot, "The Properties of Ni-Al Bronze Sand Cast Ship Propellers in Relation to Section Thickness," *International Shipbuilding Progress*, vol. 34, p. 112-123, 1987.
- [2] M.D. Fuller, "Friction Stir Processing and Fusion Welding in Nickel Aluminum Propeller Bronze," M.S. thesis, Naval Postgraduate School, Monterey, CA, 2006.
- [3] S. Kou, *Welding Metallurgy*, 2nd Ed., Hoboken, NJ: J. Wiley, 2003, pp. 370.
- [4] M.W. Mahoney and S.P. Lynch, "Friction Stir Processing." Retrieved October 2009, from http://www.darpa.mil/dso/thrusts/matdev/fsp/pdfs/fspsem_a1.pdf.
- [5] K. Oh-Ishi and T.R. McNelley, "The Influence of Friction Stir Processing Parameters on Microstructure of As-Cast NiAl Bronze," *Metallurgical and Materials Transactions*, vol. 36A, p. 1575-1585, 2005.
- [6] R.S. Mishra and Z.Y. Ma, "Friction Stir Welding and Processing," *Materials Science and Engineering*, vol. 50, p. 1-78, 2005.
- [7] E.A. Culpan and G. Rose, "Microstructural Characterization of Cast Nickel Aluminum Bronze," *Journal of Materials Science*, vol. 13, p. 1647-1657, 1978.
- [8] E.A. Culpan and G. Rose, "Corrosion Behavior of Cast Nickel Aluminum Bronze in Sea Water," *British Corrosion Journal*, vol. 14, p. 160-166, 1979.
- [9] ASTM Standard B148, 1997 (2009), "Standard Specification for Aluminum-Bronze Sand Castings," ASTM International, West Conshohocken, PA, 2006, DOI: 10.1520/B0148-97R09, www.astm.org.
- [10] K. Oh-Ishi and T.R. McNelley, "Microstructural Modification of As-Cast NiAl bronze by Friction Stir Processing," *Metallurgical and Materials Transactions*, vol. 35A, p. 2951-2961, 2004.
- [11] F. Hasan, G.W. Lorimer, and N. Ridley, "Crystallography of Martensite in a Cu-10Al-5Ni-5Fe Alloy," *Journal de Physique*, vol. 43, p. C4-653-658, 1982.
- [12] A. Jahanafrooz, F. Hasan, G.W. Lorimer, and N. Ridley, "Microstructural Development in Complex Nickel-Aluminum Bronzes," *Metallurgical Transactions*, vol. 14A, p. 1951-1956, 1983.
- [13] D.M. Lloyd, G.W. Lorimer, and N. Ridley, "Characterization of Phases in a Nickel-Aluminum Bronze," *Metals Technology*, vol. 7, p. 114-119, 1980.

- [14] F. Hasan, A. Jahanafrooz, G.W. Lorimer, and N. Ridley, "The Morphology, Crystallography, and Chemistry of Phases in As-Cast Nickel-Aluminum Bronze," *Metallurgical Transactions*, vol. 13A, p. 1337-1345, 1982.
- [15] B.P. Rosemark, "Friction Stir Processing Parameters and Property Distributions in Cast Nickel Aluminum Bronze," M.S. thesis, Naval Postgraduate School, Monterey, CA, December 2006.
- [16] S. Swaminathan, K. Oh-Ishi, A.P. Zhilyaev, C.B. Fuller, B. London, M.W. Mahoney, and T.R. McNelley, "Peak Stir Zone Temperatures During Friction Stir Processing," to be published at a later date.
- [17] K. Oh-Ishi, A. Zhilyaev, and T.R. McNelley, "A Microstructural Investigation of Recrystallization during Friction Stir Processing of As-Cast NiAl Bronze," *Metallurgical and Materials Transactions*, vol. 37A, p. 2239-2251, 2006.
- [18] M.D. Fuller, S. Swaminathan, A.P. Zhilyaev, and T.R. McNelley, "Microstructural Transformations and Mechanical Properties of Cast NiAl Bronze: Effects of Fusion Welding and Friction Stir Processing," *Material Science and Engineering*, vol. 463, p. 128-137, 2007.
- [19] M.W. Mahoney, W.H. Bingel, S.R. Sharma, and R.S. Mishra, "Microstructural Modification and Resultant Properties of Friction Stir Processed Cast NiAl Bronze," *Materials Science Forum*, vol. 426-432, p. 2843-2848, 2003.
- [20] R.A. Williams, "A Microstructural and Mechanical Property Correlation of Friction Stir Processed Nickel Aluminum Bronze," M.S. thesis, Naval Postgraduate School, Monterey, CA, September, 2004.

INITIAL DISTRIBUTION LIST

1. Defense Technical Information Center
Ft. Belvoir, Virginia
2. Dudley Knox Library
Naval Postgraduate School
Monterey, California
3. Engineering and Technology Curricular Office, Code 34
Naval Postgraduate School
Monterey, California
4. Professor Terry R. McNelley, Code ME/Mc
Naval Postgraduate School
Monterey, California
5. Professor Sarath Menon
Naval Postgraduate School
Monterey, California